Towards molecular transistors

Master thesis by Augustinus (Stijn) Marius Goossens

university of groningen

faculty of mathematics and natural sciences

zernike institute for advanced materials

Towards molecular transistors

Master thesis by Augustinus (Stijn) Marius Goossens

Abstract
A transistor made with self-assembling molecules could overcome the size limits in chip fabrication imposed by photolithography. The device concept of a metal-insulator-metal-insulator-metal (MIMIM) transistor is very suitable to incorporate self-assembled monolayers of molecules as functional elements. The objective is to fabricate a molecular MIMIM transistor with a collector barrier consisting of a conjugated molecule, quaterphenyldithiol, using large area molecular junction processing techniques. To reach this goal we had to take up several challenges. First of all we characterized electronic transport through oligophenyldithiols of two, three and four phenyl rings and found an exponential decay constant of 0.294 $Å^{-1}$. Secondly, we had to make a thin gold layer to enable ballistic charge transport across the base layer of the device. The transistor we realized in the end is not suitable as a functional switching device, but the results obtained point towards the enormous capacities of the molecular MIMIM transistor as an analytical tool to study energy level dependent transport across molecules.

TopMaster Nanoscience

University of Groningen, Zernike Institute for Advanced Materials

Group: Molecular Electronics – Physics of organic semiconductors

Group-leader: Prof. Dr. Ir. P.W.M. Blom

Supervisors: Dr. B. de Boer and Drs. A.J. Kronemeijer

Referent: Prof. Dr. Ir. B.J. van Wees

Period: September 2007 – July 2008

Table of contents

1 Introduction 3

2 Principles and considerations 6

2.1. MIMIM Operation principles 6
2.2. Hot electron energy loss mechanisms 7
2.3. Design considerations 8
2.4. Molecular MIMIM design 10
2.5. MIMIM as electron energy spectrometer 12

3 Towards a functional MIMIM 14

3.1. Collector barrier: conjugated molecules 14
3.2. Emitter barrier: SiO_2 20
3.3. Base layer: ultrathin Au 22

4 MIMIM functionality 25

5 Conclusions/outlook 29

6 Acknowledgements 30

7 Bibliography 31

8 Appendices 34

Appendix A : Large Area Molecular Junction processing 34
Appendix B : Oligophenyldithiol SAM formation 36
Appendix C : Thermal oxidation of silicon 38
Appendix D : Thin Au layer formation 40
Appendix E : MIMIM Processing 42
Appendix F : MIMIM symbol 44

1 Introduction

In the ongoing search for faster electronic circuits the main focus is downscaling of device size. But at a certain point further miniaturization of conventional semiconductor devices would dramatically increase their resistance. Another disadvantage of conventional semiconductor devices is their horizontal topography. They are manufactured using UV-lithography or maybe even electron beam lithography, but a resolution smaller than 10 nm seems impossible. A logic change in device topography would be to go vertical. When evaporating techniques are used, layer thicknesses can be controlled up to the lattice parameter length scale.
As the storage time of minority carriers is a speed limitation in a conventional bipolar transistor, a unipolar device would be an improvement. The transport mechanism in conventional transistors is diffusion, so the use of high velocity carriers could be another solution in the search for speed. A device structure that incorporates vertical topography, unipolarity and high velocity carriers is the tunneling hot carrier transistor (THCT), first proposed by C.A. Mead in 1960.[1] In this device a tunneling barrier is used as an electron launcher that abruptly accelerates the tunneling electrons from the emitter to the base. The device consists of a stack of three electrodes, with all electrodes separated by a very thin insulator, creating a metal-insulator-metal-insulator-metal (MIMIM) transistor. The device was expected to have a superior frequency performance of up to 3 TeraHz. Besides being very attractive for high speed electronic applications, THCTs can be used as spin transport devices since spin of an electron is conserved while tunneling.[2] Another nice feature of THCTs is the occurrence of negative differential resistance, an effect that can be used to make logic circuits with very few components.
Mainly due to the bad quality of both the metal and the insulating layers of MIMIMs made in the past, results were discouraging and the research in this area almost stopped. Recently, a group from Japan used lattice matched materials for barriers and contacts which resulted in an outstanding performance.[3] This device is encouraging for future work on MIMIMs, although it is not trivial making lattice matched molecular beam epitaxy structures. Fortunately, recent advances in nanoscience have led to the development of techniques and materials to give the MIMIM a prosperous future.
We believe the way to construct MIMIMs is to use the technique of self-assembled monolayers (SAMs) to make energy barriers of insulating molecules. SAMs are organic assemblies formed by the absorption of molecules from solution or the gas phase onto the surface of solids (metals). Self assembly is a very promising bottom-up nanofabrication technique because of nature's spontaneous drive to find equilibrium in creating nanostructures. The single molecule thick structure (monolayer) will just form by itself. The ease of processing and the freedom in materials, both substrates and molecules, make the technique even more attractive.
Recently, researchers at the Zernike Institute for Advanced Materials (Groningen), in collaboration with Philips Research Laboratories Eindhoven, discovered how to electrically contact a SAM by using a device structure called large-area molecular junction, shown schematically in Figure 1[4]. This large-area molecular junction is basically a MIM structure with a self-assembled monolayer of alkanedithiols as insulating barrier. The challenge is to construct two of these junctions on top of each other, and if this is done, in principle, the molecular MIMIM transistor is realized.

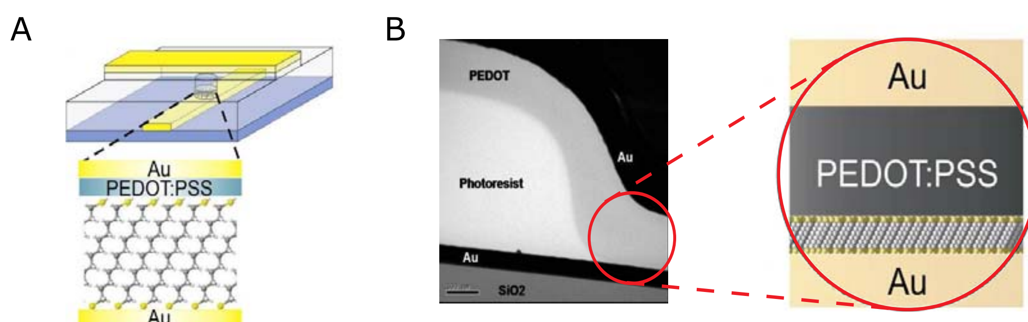

Figure 1 *(A) Large-area molecular junction: the self-assembled monolayer of alkanedithiol molecules on gold bottom contact topped with a layer of conducting polymer (PEDOT:PSS) to prevent gold from penetrating the monolayer.[4] (B) SEM micrograph of a large-area molecular junction, with a schematically magnified overview of the junction.*

To be able to build a molecular MIMIM we need more understanding of charge carrier transport through molecular junctions. Over the past decade substantial advances have been made in the field of molecular electronics. Not only molecular device functionality has been demonstrated, but also different experimental approaches to measure electron transport through molecular junctions and theoretical models to describe electron transport properties have been developed. Next to that characterization techniques to relate experiments to theory have emerged. Present understanding of charge carrier transport through molecular devices is direct (nonresonant) tunneling thought to be dominated by the height and width of the barrier resulting from the presence of molecules between the electrodes. The height of the barrier is given by the difference between the Fermi level of the electrodes and the highest occupied molecular orbital (HOMO) and/or the lowest unoccupied molecular orbital (LUMO). In principle the position of these levels can be determined by ultraviolet photoemission spectroscopy (UPS) and inverse photoemission spectroscopy (IPES). A large disadvantage of this technique is that measurements cannot be performed on molecules buried between two electrodes. The electrodes probably strongly influence the position of the molecular levels due to mixing of the wavefunctions of the electrons in the molecules and electrons in the electrodes. The wavefunction mixing depends on the coupling of the electrodes to the molecule.
To be able to characterize the junction we need an in situ measurement technique. Inelastic tunneling spectroscopy (IETS) is performed on molecules between electrodes and measures the coupling between tunneling charge carriers and molecular vibrations.[5] With FTIR on buried molecular interfaces the same can be done without the disadvantages of IETS like poor spectral resolution, low temperature requirement and the unavoidable coupling of the spectroscopic measurement to transport.[6] Unfortunately these two methods do not give us much information relevant to MIMIM transistors as nothing can be said about energy barriers. The most simple in situ measurement to determine barrier height is to do a 2-terminal I-V measurement and fit the data with the Simmons model for direct tunneling transport.[7,8] From this fit the barrier can be determined if the electron effective mass during tunneling is known. A more direct approach would be to determine the Fowler-Nordheim transition voltage. This voltage relates directly to the barrier height and the method can even be used to determine the contact asymmetry.[9] Two terminal methods suffer from image potential effects, so an external, third electrode is highly desired. Cyclic voltammetry employs a third electrode in an electrolyte to measure the oxidation and reduction potential of a molecule in a junction. The first oxidation potential relates to the HOMO of the molecule. Quinn and coworkers have found that the conductivity of molecules relates inversely with the first oxidation potential.[10] Probably the most versatile method to

determine barrier heights is ballistic electron emission microscopy (BEEM) employed by W. Li and coworkers.[11] A third electrode in the form of a STM tip fires ballistic carriers with a predefined excess energy to molecules embedded in a junction. The fact that the molecular MIMIM is very similar to the BEEM setup and work on monolithic semiconductor hot electron transistors gave us the idea to use the molecular MIMIM as a tool to determine barrier heights.

Realizing a molecular MIMIM has a twofold goal. We will not only develop a totally new transistor concept, but also a very powerful analytic tool. With the MIMIM we will be able to determine the energy level dependent transport through molecular junctions. The versatile large-area molecular junction testbed gives us the ability to do systematic studies on series of molecules. By injecting ballistic charge carriers we could even determine both the position of the HOMO and LUMO level directly and thereby answer the question if molecular transport is HOMO or LUMO mediated.

2 Principles and considerations

2.1. MIMIM Operation principles

The key elements of the MIMIM transistor are the two insulating layers. The first insulating layer serves as an electron injector and accelerator, whereas the second insulating layer acts as an electron selector that is sensitive to the energy of the incident electrons. Suppose two metals are connected with an energy barrier in between. If the barrier is thin enough the wave functions of the electrons at the interface extend into the other metal. So the electrons have a certain probability to end up at the other side of the barrier, which is called tunneling. When a bias is applied to the metals a net tunneling current starts flowing. In a MIMIM transistor this tunneling principle is used to inject electrons from the emitter into the base (Figure 2A). The tunnel junction generates a beam of electrons with an energy distribution around E_{FE} (Fermi energy level of the emitter) in the base. This beam consists of hot electrons: electrons with an energy more than a few kT higher than the Fermi level. This in contrast with cold electrons: electrons which have an energy comparable to the Fermi energy. The electrons in this beam have a very high velocity because they are accelerated by a field V_{be}/d_{be} (with d_{be} the base emitter barrier thickness) when they tunnel through the barrier. A bias V_{bc} accelerates the hot electrons to the collector and if the electrons have an energy high enough to surmount the base-collector barrier $\Phi_{C,}$ the electrons can flow into the collector. With this last element, a three terminal device is completed.

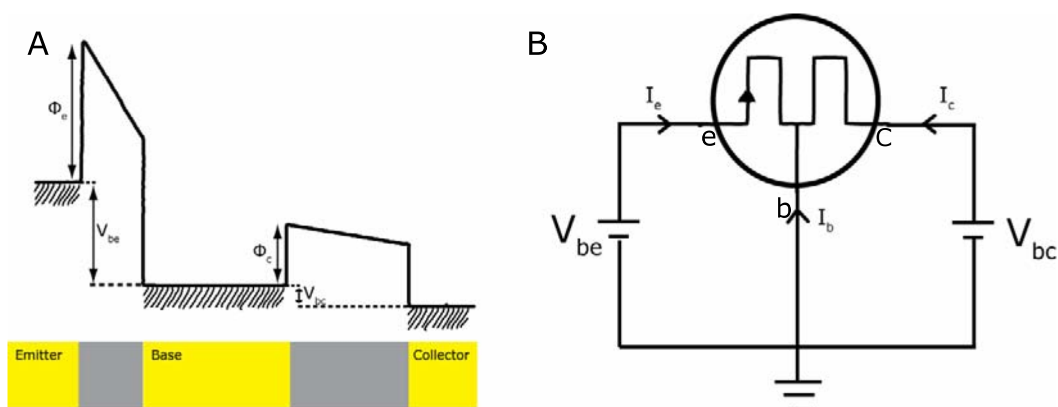

Figure 2 *(A) Energy diagram of the tunnel transistor with symbol labeling. Below a schematically depiction of the MIMIM concept: in yellow the metal contacts and in grey the insulators. A one dimensional model applies since the linear dimensions are much smaller than the other dimensions (B) Common base connection circuit with definition of current directions and voltage labels. For an explanation of the MIMIM symbol, see Appendix F.*

If $V_{be} < \Phi_C/e$ (Figure 3A and B) the hot electrons bounce back off the base-collector barrier and thermalize in the base, resulting in $I_E=-I_B$. This is the off-state of the transistor. Biasing the collector positively ($V_{bc}>0$) will leave the barrier height unaffected (neglecting the image charge correction) and the observed collector current will result only from tunneling electrons from the base. To minimize this current, the collector barrier has to be thick enough to prevent tunneling.
The collector current will suddenly rise when V_{BE} exceeds $\Phi_C/e - \delta$ (Figure 3C), provided the energy distribution of the tunneling electrons is characterized by δ, half the normal energy spread of the electron beam energy distribution. This is the on-state of the device. The input power for switching the output of the device in common base configuration will be small (directly proportional to δ^2, which is temperature and device parameter sensitive).

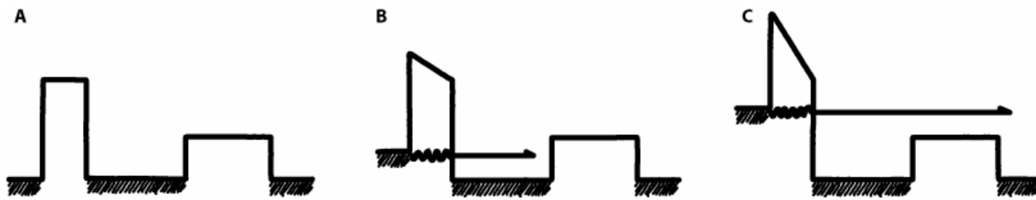

Figure 3 *Energy banddiagrams of different biasing regimes of the MIMIM. (A) $V_{be}=0$, no current flowing in the device. (B) $V_{be} < \Phi_C/e - \delta$, injected electrons thermalize in the base, off-state (C) $V_{be} > \Phi_C/e - \delta$, injected electrons can surpass the second barrier, on-state.*

2.2. Hot electron energy loss mechanisms

Due to loss processes, only part of the injected hot electron current (I_e) is collected by the collector. This leads us to define the transfer ratio $\alpha=-I_c/I_e$, using the convention of $I>0$ when the current flows into the port and I_c the collector current. Notice that α is also referred to as the 'common base' current gain, so it is an important figure of merit for functionality of the device, both in amplifier applications and in spectroscopic applications. There are several loss mechanisms possible in the MIMIM transistor. In reference [12] these mechanisms are thoroughly revised. Here we summarize them very briefly:

Quantum mechanical spread of tunneling electron current: As already mentioned in paragraph 2.1 the beam of injected electrons is not mono energetic but has a certain energy spread characterized by δ. Heiblum calculated this spread and determined that the energy distribution has a large tail below the Fermi level of the emitter contact.[13] Not all electrons will be collected when the peak of the electron energy distribution is already above the collector barrier, resulting in a decrease of transfer ratio.

Collisions in the conduction band of the base emitter barrier: If the emitter-base barrier is strongly biased ($eV_{BE} > \Phi_E$), tunneling electrons spend part of their path in the conduction band of the emitter barrier. This conduction band is a very strong scatterer.

Scattering of hot electrons in the base: The mean free path (mfp) is a measure for the amount of scattering of hot electrons in the base. It can be estimated using the formula $\alpha=\exp[-d_b/mfp]$, where d_b is the base thickness and α the transfer ratio of the device. The most important point to remember about the mean free path is its

decrease with increasing excess energy. In metals, mechanisms that cause hot electron scattering are: electron-defect or electron-impurity, electron phonon and electron-electron collisions.

Quantum mechanical reflection from the base collector barrier interface: Classically, electrons impinging on a barrier are not reflected if their energy exceeds the barrier height. But quantum mechanically, there is always a finite reflection above the barrier which decreases as the electron excess energy above the barrier increases. In Figure 4 depicts the reflection as function of electron energy for a simple rectangular barrier.[14]

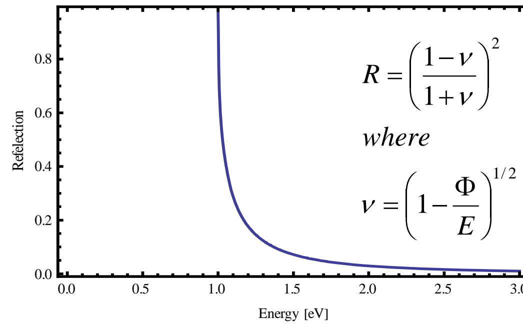

Figure 4 *Quantum mechanical reflection plotted as function of energy for a barrier of 1 eV. The reflection is as high as 25% for an excess energy of 0.125 eV over the barrier.*

The effective mass on each side of the barrier is also strongly influencing the transmission, which can be expressed as:

$$T = \left(\frac{A_t}{A_i}\right)^2 \frac{m_i^*}{m_t^*}$$

With A the amplitudes of the wave functions, m^* the effective mass. I and t stand for the medium of incidence and transmission respectively.

Collisions in the conduction band of the base-collector barrier: If the energy of the electrons is higher than the barrier height, electrons will pass the barrier. When the energy gets higher and higher, the number of generated optical phonons will increase and the transmission will diminish.[13] Fortunately this effect will not degrade the transfer ratio very much, because we can apply some collector bias to collect almost all electrons that lose energy in the conduction band of the collector barrier.

Quantum mechanical reflections from the collector barrier- collector interface: Classically, no reflections occur at this boundary, but quantum mechanically they do occur. These reflections only contribute few tens of percents.[13]

2.3. Design considerations

In the previous paragraph, we reviewed theoretically all relevant loss mechanisms for ballistic electrons in MIMIM transistors. To achieve a good performing MIMIM we have to minimize these loss mechanisms. Next to that we have to take into account some design rules for tunneling hot electron transistors.

The basic requirements for operation of a MIMIM are:
(a) $r_{out} >> r_{in}$ to achieve power gain (r_{out} is the output resistance and r_{in} is the input resistance)

(b) τ_{in} and τ_{out} as small as possible for high frequency performance (τ_{in} is the input transit time and τ_{out} is the output transit time)
(c) maximize α

Requirement (a) (high collector impedance) is easily satisfied if the thickness of the collector barrier is much larger than the thickness of the emitter barrier. Condition (b) requires small area devices. Small area devices have another advantage: a thin emitter barrier layer is enough to achieve an impedance high enough to overcome problems with the base spreading resistance. If the collector barrier is low enough (preferably ~0.5 eV), V_{be} can be small. This has on one hand the advantage that operation in the Fowler-Nordheim regime of the emitter junction can be prevented, which results in a much lower excess energy of the electrons in the base and reduced scattering in the emitter barrier. On the other hand reflections will diminish faster for a low collector barrier as they are dependent on the relative distance of the electron energy to the barrier. Both effects will result in a higher transfer ratio: requirement (c).

Heiblum has predicted the performance of a MIMIM amplifier.[13] The main result of his calculations is the requirement of a relatively low and thick emitter-base barrier. But the emitter-base barrier should of course not be lower than the collector barrier. The first reason for this result is the fact that the energy distribution of the emitted electrons is most narrow for $V_{be}= \Phi_e/e$ and a thick layer. The second reason results from the first, because having a low emitter barrier means the charge carriers will not have a high excess energy in the base when the device is operated at $V_{be}= \Phi_e/e$. The calculations were based on an ideal structure, in practice even more difficulties are encountered:

-Non-tunneling current: transfer of electrons through pinholes and metallic microbridges in the barrier.
-Inelastic tunneling: interactions of electrons with resonance centers in the barriers.
-Barrier impurities and traps: imperfections change locally the barrier height which is especially important for the collector barrier. Traps will reduce the collected current.
-Base pinholes: electrons transfer through the base, without being affected by the base voltage.
-Base spreading resistance: the base spreading resistance should be much smaller than r_{in} to avoid V_{be} being dependent on the base current. The spreading resistance increases when the base is made thinner.
-Skin effects in the base: high frequency operation will lead to coupling between collector and emitter.
-Interface states: interface states could act as trapping centers and reduce the transfer ratio.
-Geometrical realization of signal coupling: since the areas of the devices are small, some kind of a high frequency signal concentrator (antenna) is needed to guide energy into the device.

Some MIMIM transistors are already realized. Although researchers knew the design parameters, they could not implement them very well as they were limited by the fabrication techniques at that time. Table 1 summarizes the results and parameters of the devices.

Emitter metal	*E-B barrier*	*E-B barrier thickness [Å]*	*Base metal*	*Base thickness [Å]*	*B-C barrier*	*B-C barrier thickness[Å]*	*Collector metal*	*α_{max}*	*Ref*
Al	Al_2O_3	70	Al	100	SiO	100	Al	0.1	15
Al	Al_2O_3	40	Al	200	Al_2O_3	50	Al	0.02 (77K)	16
Al	Al_2O_3	33	Al	150	Al_2O_3	33	Al	0.01 (77K)	17
Al	Al_2O_3	100	Al	130,150	Al_2O_3	100	Al	.26, .2(300K)	18,19
$CoSi_2$	CaF_2	19	$CoSi_2$	19	CaF_2	50	n-Si (10^{22} cm^{-3})	0.94 (β=36)(77K)	3

Table 1 *Parameters and performances of realized MIMIMs*

Disappointing performances (low α) of the first MIMIMs were first appointed to the reflections from the base-collector barrier, but the $CoSi_2$-CaF_2 MIMIM proves the contrary. Although this device has almost square barriers, the transfer ratio is very high, due to the good quality of the insulating CaF_2 films. So, the low transfer ratio of the MIMIM transistors was probably caused by the bad quality of the oxide insulating layers. Still, the main loss mechanism in a MIMIM with good barriers could be the reflections from the base-collector barrier. So graded barriers could be a good improvement. A new development in the area of THCTs also points in this direction. Chao and coworkers have developed a polymer tunneling hot carrier transistors with a very high common emitter current gain at room temperature.[20] Because the polymers are not crystalline, the base-collector interface is 'soft' and almost no reflection from the barrier occurs. These results suggest that future research on THCTs should focus more on the use of organic materials.

2.4. Molecular MIMIM design

In this thesis we will try to create a MIMIM transistor with self-assembled monolayers (SAMs) as insulating barriers. SAMs have several advantages over conventional insulating layers and incorporating a SAM in the collector barrier of a MIMIM will allow us to study the energy level dependent transport through the molecules. The main MIMIM problems encountered in the past were due to the bad quality of the insulating oxide layers. SAMs will probably contain fewer defects than oxide layers since there are no problems with lattice matching: SAMs order themselves on the substrate. Another advantage of SAMs over conventional oxides is their engineerability. Chemists can synthesize self assembling molecules with almost any length and HOMO-LUMO gap (related to barrier height). This in contrast to oxides: they have a nearly fixed barrier height and the thickness can only be varied within certain limits. If you make the oxide too thin a high chance of pinhole formation exists, but if the oxide is too thick, to prevent pinhole formation, no tunneling current flows.

A structure for the molecular MIMIM has to be devised. We need to find a way to stack two self-assembled monolayers of insulating molecules, separated by a thin metal electrode, the base. There are several routes to construct a molecular MIMIM with a thin base layer. One possibility is to stamp the thin base layer directly on the SAM with a PDMS stamp, using a technique called Nanotransfer printing.[21] On this stamped gold layer we will assemble the second monolayer of molecules. The contact to this second layer of molecules will be the PEDOT:PSS top contact of a large-area molecular junction[4]. Figure 5A is a schematic overview of the structure of this design.

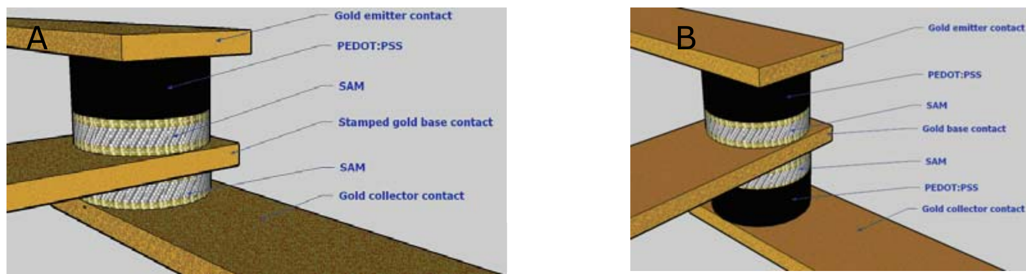

Figure 5 *(A) Structure of the stamped base MIMIM. (B) Structure of the flip-over MIMIM. Compared to Figure 1 this structure uses two mutually connected large-area molecular junctions*

The second possible route is to use two large-area molecular junctions mutually connected through their bottom contacts (Figure 5B). This requires the ability to remove the large-area molecular junction from its substrate and to process another large-area molecular junction on the bottom of the first device. Possibly this can be realized by using a method called template stripping[22].

These two elegant approaches are major technological challenges. For the stamped base approach we have to develop an entirely new molecular contact technique and these molecular junctions have to be resistant against the solvent for the next self-assembled monolayer, to name just two of the difficulties. To connect two large-area junctions mutually is maybe even harder since we have to devise a way to reach the bottom of the bottom contact of the first molecular junction.

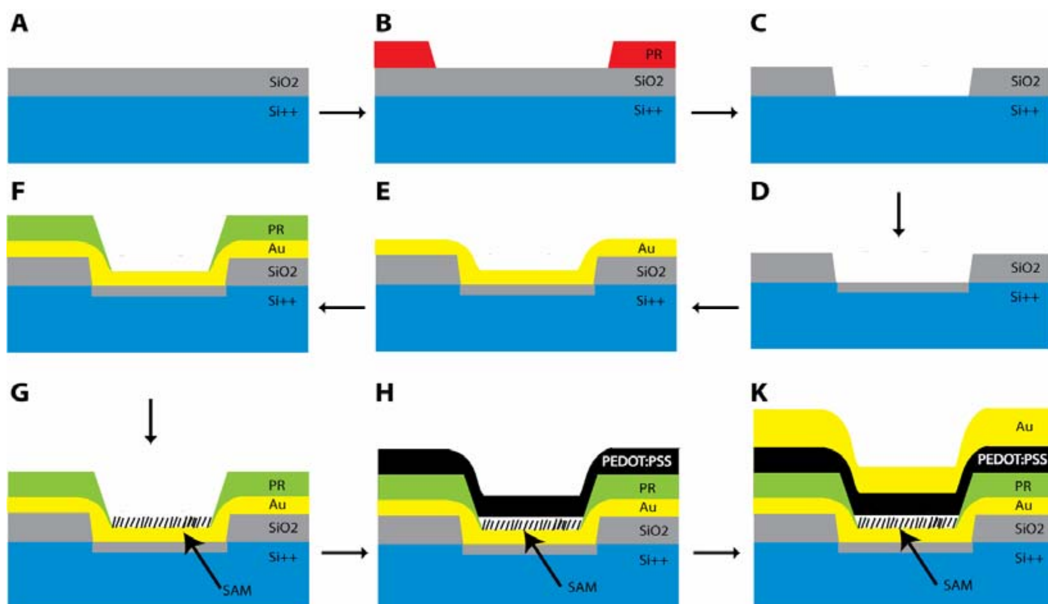

Figure 6 *Flowchart for processing a MIMIM transistor with a SiO_2 emitter barrier. (A) Starting point is a silicon n^{++} wafer with 500nm oxide (B) Spincoat positive photoresist, expose and develop to define via holes for the emitter barrier (C) Etch the SiO_2 away and remove the photoresist (D) Grow an ultra-thin layer of oxide by thermal oxidation (E) Evaporate a thin layer of Au as base layer (F) Spincoat negative photoresist, expose and develop to define via holes for the collector barrier (G) Put the wafer in a SAM solution to create the collector barrier with molecules. (H) Spincoat PEDOT:PSS (K) Evaporate Au as collector contact.*

Due to these difficulties we have chosen to first try to test the concept of self-assembled monolayers as barriers in a MIMIM transistor. We will not develop a MIMIM transistor with two SAMs, but just one. The other tunnel barrier will be a silicon oxide barrier, which is easier to implement in the design. Standard highly doped silicon wafers can be used simultaneously as substrate and electrode on which a silicon oxide layer is thermally grown, creating the MI. The final MIM stack is processed using conventional technology for large-area molecular junctions.[4] In Figure 6 we have drawn a schematic flowchart for creating a SiO_2 emitter barrier. In Appendix E we have written down the detailed processing scheme for this MIMIM.
In this chapter we have only determined the materials and processing steps needed to make a SiO_2 emitter barrier molecular MIMIM. We did not comment on, for example, the thickness of the SiO_2 and Au base layer, neither on the choice of the molecule in the collector barrier. The paragraphs of chapter 3 are devoted to the development and characterization of the separate elements of the MIMIM.

2.5. MIMIM as electron energy spectrometer

In the previous paragraphs of chapter 2 we discussed the physical mechanisms underlying the workings of the MIMIM transistor and possible routes to realize a MIMIM transistor with molecules. Because a fully molecular MIMIM is an enormous technical challenge we will first determine if molecules (SAMs) are suitable as energy barrier in a MIMIM transistor. To do this we will use the device as a versatile testbed to study charge transport properties of all kind of different molecules.
According to the paper published by W. Li and coworkers[11] on ballistic electron emission microscopy (BEEM) we should be able to use the MIMIM as an analytic tool to determine the barrier height of a molecule in our junctions. In stead of an STM-tip emitter electrode and a vacuum barrier we use a Si^{++} emitter electrode and a SiO_2 barrier to launch ballistic electrons with a specific electron excess energy determined by the emitter-base voltage. Also in the field of tunneling hot carrier transistors the idea to do electron energy spectroscopy with the devices is already deployed. Heiblum and Fischetti studied ballistic transport through monolithic semiconductors with a MIMIM-like device.[23] They used the collector barrier as a high pass filter to extract the electron energy distribution after the electrons traversed the base made of monolithic semiconductor. We do not want to study ballistic transport through the gold base layer, but we want to know the barrier height of the molecules in the collector junction.
The current density (J) at an applied voltage (V) can be expressed as $J(V) = e\int n(E_\perp)v_\perp(E)dE_\perp$ (n(E) is the electron density distribution and v(E) the electron velocity distribution). When we put a barrier Φ in the way of the electron beam the current density behind the barrier is $J(V) = e\int_\Phi^\infty n(E_\perp)v_\perp(E)dE_\perp$ as we show in Figure 7.

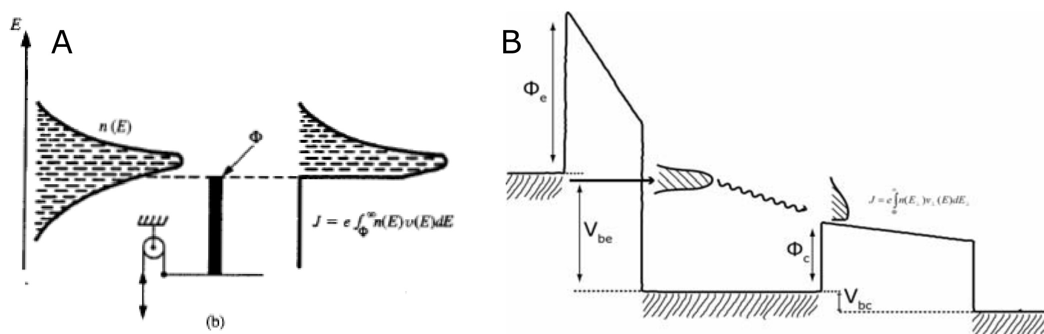

Figure 7 *(A) High pass filter electron energy spectrometer. On the left the incident electron energy distribution, in the middle the barrier Φ that can be altered and on the left the current distribution behind the barrier together with the expression for the measured current density of the collector.[23] (B) Application of the electron spectrometer concept in the MIMIM. The wavy arrow symbolizes the energy losses in the base.*

Conventional MIMIM spectroscopy experiments determined $n(E_\perp)v_\perp(E)$ by calculating dJ/dΦ with Φ the collector barrier height varied by the base collector voltage (V_{bc}) as proposed by Hesto and coworkers[24] (Figure 7A). In contrast, we want to know the height of the collector barrier relative to the Fermi level of the base. Therefore we do not need to vary V_{bc}, but V_{be}. When the injected electron beam is mono-energetic and no losses occur, the collector current shows a step when the electrons have an energy that equals the collector barrier height, so exactly at $V_{be}=\Phi_c$. In this way we will be able to determine the barrier height of the molecule by a direct measurement.
Of course in reality the electron beam is not mono-energetic due to the loss mechanisms described in paragraph 2.2. Both the energy spread δ and the mean excess energy of the beam are affected by scattering in the base. This results in a measurement error in the exact barrier height, because the applied emitter voltage does not exactly correspond to the excess energy of the electrons have when they arrive at the collector barrier (schematically shown in Figure 7B by the wavy arrow). Another major effect that induces an error in the measured barrier height is the quantum mechanical reflection from the barrier. Both these effects result in a measured barrier height that is larger than the real barrier height. To make a measurement as precise as possible we need to maximize the transfer ratio α. Unfortunately, we can not avoid quantum mechanical reflections and as these reflections will possibly differ from molecule to molecule they will seriously affect the viability of this method to determine molecular barrier heights.

3 Towards a functional MIMIM

3.1. Collector barrier: conjugated molecules

For the molecular MIMIM we need long molecules with a low HOMO-LUMO gap to satisfy requirement (a) in paragraph 2.3. In this paragraph we will test several candidates for their suitability to function as collector energy barrier in the MIMIM and at the same time for their abilities as molecular wire.

In the introduction we pointed out that the molecular MIMIM is a good candidate to be the successor of the current silicon transistor. The molecular MIMIM could be the first adept of an entirely new technology field called molecular electronics. Many scientists believing in molecular electronics dream of a computer chip built entirely with molecules. To make this happen they need not only functional elements like the Aviram & Rattner diode-molecule[25] or an optically switching molecule[26], but also insulators to prevent parasitic currents and wires to connect the functional elements. Insulating molecules are for example simple alkanes. To make molecular wires, we require conducting molecules. As direct tunneling is the transport mechanism widely assumed for insulating molecules, we need to lower the energy barrier induced by the molecule to increase the tunneling current. If the energy barrier gets even lower, the main charge transport mechanism through the molecule is hopping.[27] Lowering the energy barrier of a molecule basically means lowering the HOMO-LUMO gap. This is not so evident as it seems, because it is not clear how the HOMO and LUMO levels of the molecule align with the metal electrodes. Lowering of the HOMO-LUMO gap means we need to increase aromaticity. We need molecules with extended π-orbitals, so long molecules with a conjugated backbone are good candidates, for example, long oligophenylene molecules used by Frisbie and coworkers.[27] We will use biphenyldithiol (P2DT), terphenyldithiol (P3DT) and quaterphenyldithiol (P4DT) (see inset Figure 11 for structures).
De Boer and coworkers measured the HOMO-LUMO gap with UV-Vis spectroscopy in solution and confirm that the oligophenyldithiols indeed have lower HOMO-LUMO gaps than alkanes (~3,5 eV optical gap compared to ~9 eV).[28] Also the increase of aromaticity with length of conjugated molecule was observed: P2DT has the largest HOMO-LUMO gap and P4DT the lowest. With the molecular MIMIM we will try to directly measure the barrier height of the molecules when they are connected between two electrodes. The results of these measurements are presented in chapter 4. But there are also other methods available to measure barrier height. In the introduction of this thesis we referred briefly to the Simmons model[29,30] for direct tunneling and the Fowler-Nordheim model[31] for field emission. These two models can both be used to extract barrier heights from 2 terminal I-V measurements. If $\Delta V<\Phi/e$ direct tunneling (Figure 8B) is the charge transport mechanism. For direct tunneling in the low bias regime the Simmons model gives the following resistance times surface (RS) dependence:

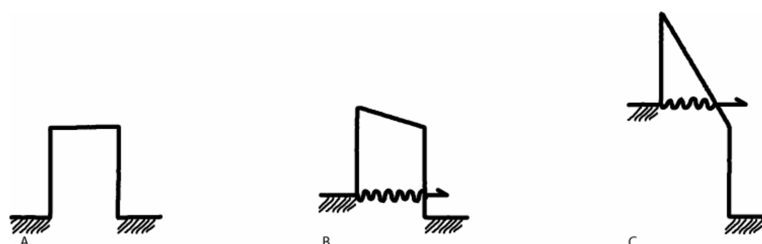

Figure 8 *Different transport regimes for different biases over a rectangular barrier with height Φ (A) ΔV=0, no charge transport (B) ΔV<Φ/e, direct tunneling (C) ΔV>Φ/e Field emission or Fowler-Nordheim tunneling.*

$$RS \propto \mathrm{Exp}[2d(2m^*_e\Phi)^{1/2}/\hbar] \quad (1)$$

With d the thickness of the barrier, m^*_e the effective electron mass, Φ the barrier height and ℏ the reduced Planck constant.
32

If we plot RS against thickness on a log scale we can extract from the slope of this plot (β) the barrier height if we know the electron effective mass:

$$\Phi = 1/(8.m^*_e)(\beta.\hbar)^2 \quad (2)$$

When the bias exceeds the barrier height, the barrier changes from trapezoidal to triangular and the field emission regime is entered (Figure 8C). Field emission is also called Fowler-Nordheim tunneling and after linearization it can be described by the following relation[9]:

$$\mathrm{Ln}(I/V^2) \propto -(4d(2m^*_e\Phi^3)^{0.5}/(3\hbar q)(1/V) \quad (3)$$

With q the electron charge and V the applied voltage bias.

So if we plot $\mathrm{Ln}(I/V^2)$ against 1/V we can extract the barrier height from the slope in the Fowler-Nordheim regime. As Beebe and coworkers pointed out also the transition point in this plot is related to the barrier height.[9]

In this experiment we want to see if the increase in aromaticity and thus possibly lowering the energy barrier indeed affects the current. So the resistance as function of length and, if possible, the energy barrier the molecule induces need to be measured. We will use large-area molecular junctions to create contacts to the molecules. So far, only electronic transport through SAMs of alkanes has been characterized in large-area molecular junctions.[4,8] Charge transport through alkanes shows direct tunneling behaviour. That is, an exponential length dependence of resistance and no temperature dependence of the current through the molecules. This exponential dependence on molecular length is quite strong due to the high energy barrier they induce and can be described by $RS \propto \mathrm{Exp}[\beta d]$ where RS is resistance times surface, β the decay constant and d the thickness of the tunnel barrier.
How we make large-area molecular juntions[4] is extensively described in Appendix A. The new challenge is how to form monolayers of oligophenyldithiols. To depict the experimental parameters for SAM formation, we summarized data found in literature in Table 5, Appendix B. The solvent used was THF and the concentration of molecules 300 μM. The self-assembled monolayers were formed in an inert environment. The oligophenyldithiols had capped endgroups (acetyl-protected) to prevent polymerization. We added 2 drops of 25% ammonia to the SAM solution to deprotect the molecules. Normally we use concentrations of 1 mM for SAM formation in our molecular junctions. But as Tour et al.[33] point out, even when working in an inert environment with acetyl-capped molecules, a high concentration can form a multilayer. For full experimental details on the SAM formation procedure, see Appendix B.

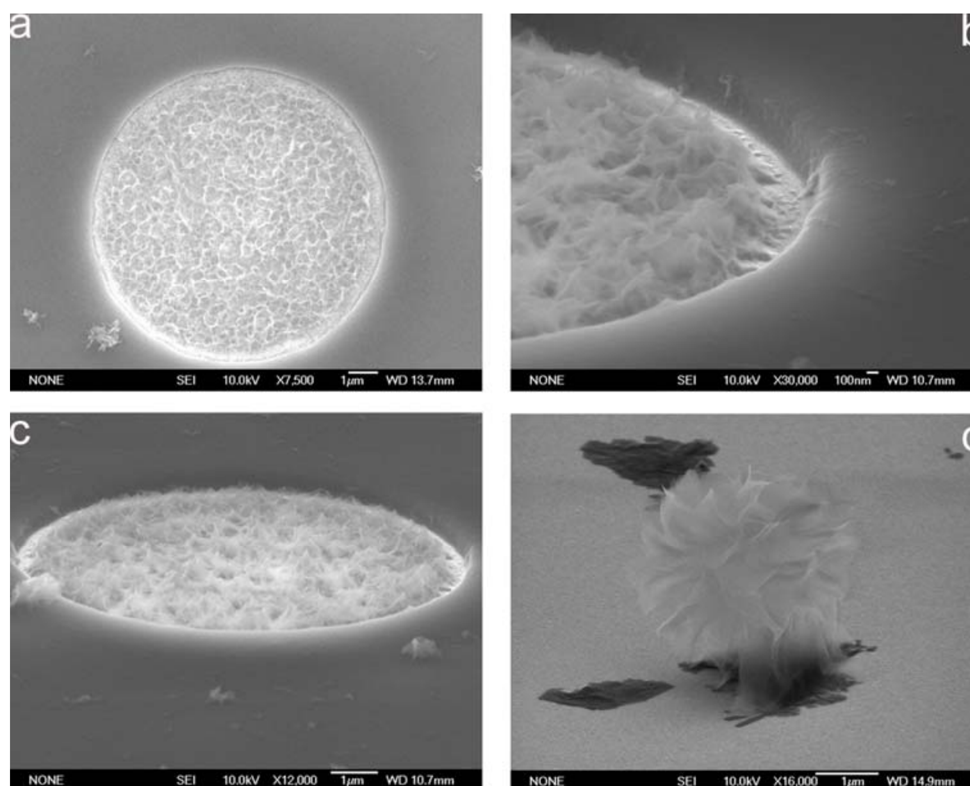

Figure 9 *SEM pictures of pores with polymerized terphenyldithiol molecules inside. SAM solution had a 1 mM concentration. a) Top view of pore, the assembly of TPDT was performed under ambient condictions b) 70 degree zoom of pore in a c) 70 degree overview of pore in a d) Gold substrate immersed in a 300 μM TPDTAc solution in a ambient environment.*

In the first experiments carried out in ambient conditions, we measured very low currents through the molecules. After close inspection of the junctions with a scanning electron microscope (JEOL JSM-7000f) we clearly saw polymer formation in the holes, even when we used acetyl-capped molecules (Figure 9). To prevent polymerization, SAM formation was carried out inside a glovebox. To check if the monolayer was really a single layer, we performed ellipsometry with a spectrometric ellipsometer (J.A. Woollam & Co V-Vase). Table 2 shows the results of the measurements. The data are in good agreement with reference [28]. Note that the (off-normal) tilt angle of the molecules decreases with molecule length as was also observed for oligothiophenes[28]. When we performed ellipsometry on oligophenyldithiol monolayers assembled in an ambient environment, the measured layer thickness was only two times higher than the values in Table 2, but it evidently demonstrated that the monolayer was not good.

Molecule	Theoretical molecule length (Å)[28]	Thickness SAM (Å)	Angle with normal (°)
P2DT	13.3	9.8 ± 1.29	43
P3DT	17.6	14.7 ± 1.67	33
P4DT	21.6	20.6 ± 0.39	18

Table 2 *Ellipsometry data of oligophenyldithiol SAMs. Wavelength range 300-500nm (BPDT 300-600nm, because of a worse fit quality value in the range 300-500 nm), angle of incidence 60°,65°,70°. n=1.55. Fitted with the following model: Si(1mm)-Cr(1nm)-Au(60nm, n&k fitted for Au reference sample)-Cauchy(thickness fitted)*

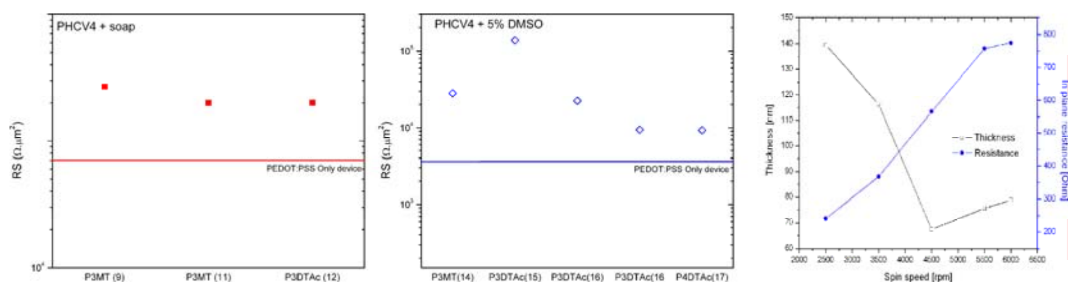

Figure 10 *Overview of RS values for wafers with conjugated molecules. The labels on the x-axis depict the type of molecule and the wafer number. The plot on the left is for Baytron PHCV4 with soap, in the middle for Baytron PHCV4 with DMSO. On the right we plot the dependence of layer thickness on spinning speed and the dependence of in-plane resistance on spinning speed and thus layer thickness.*

In Figure 10 we have summarized the resistance measurements on conjugated molecules. Figure 10b shows a similar RS-value for P4DT and P3DT, which we could explain by a limiting PEDOT:PSS resistance. Note that we even tried to increase the conductivity of the PEDOT:PSS by adding 5 vol.% dimethylsulfoxide, but without success: we still could not see a length dependence of resistance. We also tried to increase the conductivity of the PEDOT:PSS layer by lowering the layer thickness. Although the in-plane conductivity decreases (Figure 10c), the resistance of a large-area molecular junction without molecules (PEDOT:PSS only) remained the same. The resistance of the PEDOT:PSS layer in our large-area molecular junctions decreases if we decrease the bulk resistivity, but not if we decrease the in plane resistance.[†]

Assuming a good monolayer, we conclude from these data that the conjugated molecules are conducting better than alkanes, although no length dependence is observed, which would be a conclusive sign that we are measuring molecules. Because it is believed that transport through molecular junctions is factorized[34], so $G \propto T_{c1} x T_{mol} x T_{c2}$ (G the conductance and T_{c1} and T_{c2} the transmission of contact 1 and 2, respectively, and T_{mol} the transmission of the molecule) it could be possible to see a length dependence if we increase the contact resistance of the molecules. This results in an absolute value of the molecular resistance that is much higher than the PEDOT:PSS-only value. To increase contact resistance one could basically alter the bottom electrode coupling or the top electrode coupling to the molecule. The first thing we could do is decrease the roughness of the bottom electrode.[35] A second possibility is to play with the PEDOT:PSS interaction. Although a PEDOT:PSS-only device does not have a different RS value after changing the layer thickness, the interaction of the molecule with the PEDOT:PSS could be altered in a favorable way. One experiment performed on a P4DT molecule points in these directions. The RS value was a factor 10 higher than the other P4DT measurements. The molecule was assembled on a flat bottom electrode (Chapter 3.3) and the spin speed for the PEDOT:PSS layer was 6000 rpm.
We performed the same experiments also at Philips Research Laboratories Eindhoven (PRLE). Because it is possible to do 4 probe measurements on their molecular junctions we could eliminate probe contact resistance. Processing was done with the equipment of PRLE and the PEDOT:PSS used was 'Agfa ICP new type', all other experimental details were the same. The layout of their wafer and structure of the contacts is displayed in Figure 12B.

[†] *This is most likely correlated to the morphology of the PEDOT:PSS. PEDOT forms a pancake-like structure with the PSS in between.[55] The resistance of the layer is possibly determined by the ratio of the thickness of the PEDOT pancake and PSS layer, so not by the thickness of the entire layer.*

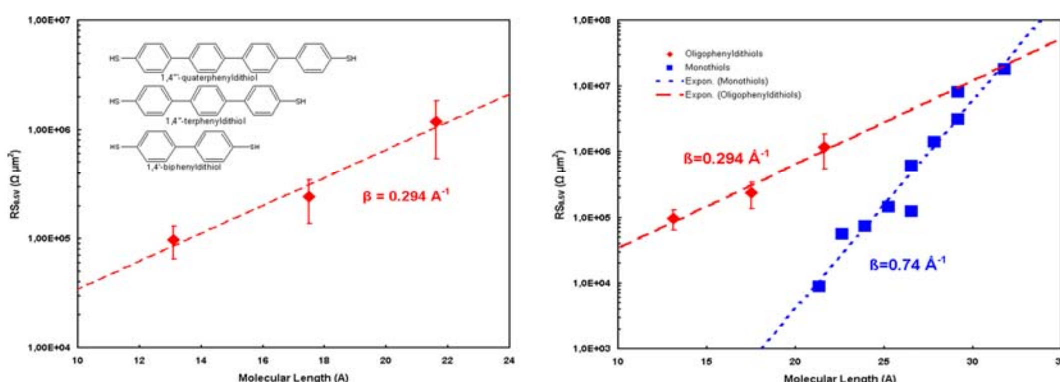

Figure 11 *RS of oligophenyldithiols plotted versus the length along the backbone of the molecule. Left: the data for the oligophenyldithiols P2DT, P3DT and P4DT. Right: the data of the oligophenyldithiols compared with alkanemonothiol data made at PRLE (Su-8 technology). We have to note that the alkanemonothiols are made on a wafer with Su-8 resist which is observed to lower the absolute RS-value with a factor 10.*

The data from these experiments are plotted in Figure 11. A decay coefficient β of 0.294 $Å^{-1}$ is extracted by an exponential fit to the data. We have plotted RS values against the length of the backbone of the molecule. If one would plot the RS values of the molecules against the measured thicknesses of the SAMs, the decay constant is 0.2. In comparison to literature this value is clearly too low, which indicates that the transport of electrons occurs along the backbone of the molecules. This was also observed for alkanes.[4] Figure 11 demonstrates that the decay coefficient is lower than for the alkanemonothiols. This could be explained by the higher electron density on the aromatic rings that makes the electron wave functions decay less. A feature we did not expect is the higher absolute RS of the oligophenyldithiols than the alkanemonothiols (Figure 11). Because of the lower energy barrier the tunneling current should be higher. Probably the coupling to the electrodes is weaker for oligophenyldithiols than for alkanemonothiols.
The β value of 0.294 $Å^{-1}$ is comparable to the value of 0.3 $Å^{-1}$ found by Frisbie and coworkers for tunneling transport through oligophenyleneimines (OPIs)[27]. Although the OPIs are also conjugated molecules they are not the same as oligophenyldithiols. Therefore it is more fair to make the comparison with other oligophenylene experiments. Frisbie and coworkers also reported AFM conductance measurements on oligophenylene thiolates which gave decay constants of 0.42 ± 0.07 $Å^{-1}$.[36] The value of 0.67 ± 0.1 $Å^{-1}$ obtained for oligophenylenethiolate SAMs by Rampi and Whitesides using Hg drop experiments on SAMs on an Ag substrate is in less correspondence with our measurements.[37] Decay constants obtained by electrochemical methods on similar aromatic SAMs are closer to our value: 0.36 – 0.57 $Å^{-1}$.[38,39] A theoretical study investigating the effect of planarity and non-planarity of the phenyl rings reports a decay constant of 0.256 $Å^{-1}$ for non-planar oligophenyldithiols.[40]

To check if the charge transport mechanism was tunneling or hopping, we performed J-V scans at different temperatures for a P4DT wafer, plotted in Figure 12A. No temperature dependence occurred which is a strong argument for direct tunneling.

Fowler-Nordheim (FN) tunneling was never observed in large-area molecular junctions, because the large HOMO-LUMO gap of alkanes and the likely damage to the junctions when applying a voltage larger than 1V. Conjugated molecules could be candidates to show FN tunneling. To clearly see the transition point to the FN regime we had to apply a voltage larger than 1V. 1.8V was determined to be the maximum, because hysteresis started to occur above this voltage. In Figure 12C we plotted a J-V curve for different areas of a P4DT wafer and in Figure 12D we show a Fowler-Nordheim plot

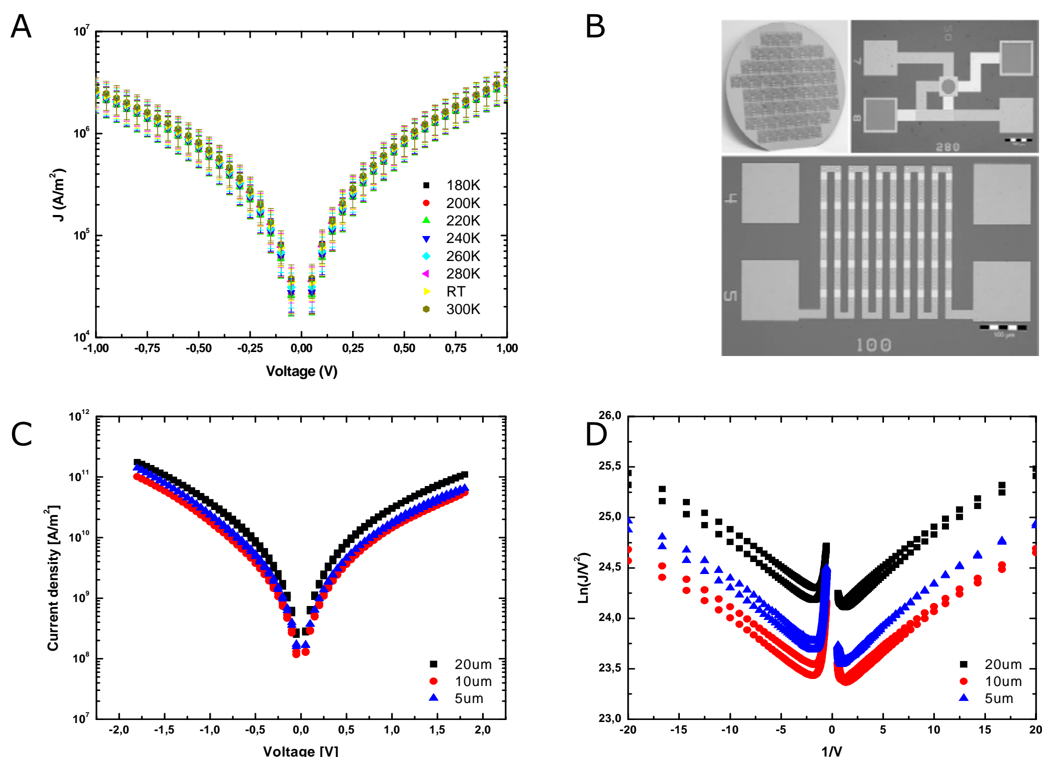

Figure 12 *(A) P4DT J-V scans for different temperatures (B) PRLE Wafer structures: top left entire wafer with 64 dyes, top right kelvin structure with via for SAM, bottom string with 100 molecular junctions. (C) P4DT molecule J-V data up to 1.8V for different device sizes. Scaling is good and almost no hysteresis occurs. (D) Fowler-Nordheim plot from the J-V data on the left.*

extracted from those J-V data. For both negative and positive bias a clear transition point is observed. The exact values for the transition points are given in Table 3. Note that P3DT did not show the entire transition to the FN regime, even with a new pulsed measurement technique that could bias the junctions up to 3V without damage. We did not measure P2DT. For tunneling from gold to PEDOT:PSS, which means negative bias, the transition occurs at a lower voltage (0.57V) than in the positive bias regime (0.85V), so the barrier is probably not rectangular.
Another method to extract the barrier height from a 2 terminal measurement is to fit the slope in the linear part of a FN plot since FN theory predicts linear dependence between $Ln(I/V^2)$ and 1/V for FN tunneling. For negative bias we clearly observe this linearity and with the help of formula (3) we can calculate the barrier height from the extracted slope. It appears to be 0.4 eV, lower than the barrier heights extracted from the transition points.
The Simmons' model fit is the last method we use to determine a value for the tunnel barrier height. With the help of formula (2), the fitted β of 0.294 $Å^{-1}$ and the effective mass taken from reference [32] we could calculate the barrier height for each molecule. The results are displayed in Table 3. It turns out that the barrier increases for increasing aromaticity of the molecule. We would not expect this as the HOMO-LUMO difference decreases for increasing aromaticity. There are many reasons to distrust this calculation. For example we do not know if the effective mass calculation is correct, as we could not find more papers with an estimate for the effective mass of electrons tunneling through conjugated molecules.

Molecule	FNT TP neg.	FNT TP pos.	FNT slope neg.	β Simmons
P2DT	-	-	-	0.44 (m^*=0.183m_0)
P3DT	-	-	-	0.47 (m^*=0.172 m_0)
P4DT	0.57±0.04	0.85±0.13	0.40±0.07	0.50 (m^*=0.161 m_0)

Table 3 *Overview of barrier heights extracted from I-V measurements on conjugated molecules in large area molecular junctions. All values are given in eV and m^* is the effective mass. For P2DT and P4DT the effective mass was calculated in reference [32]. For P3DT we estimated m^* to be in between the other two values.*

Beebe and coworkers report FN transition voltages for P1DT, P2DT and P3DT.[41] If one extrapolates the transition voltage trend with length, our value of 0.57 for P4DT fits in quite well. But we should not forget that P3DT does not show a transition to the Fowler-Nordheim regime below 3V. Other references on barrier heights for these molecules are not found, so the values we presented here can give us only a feeling for the magnitude of the barrier. If the energy barrier of the molecules is really below 1V, long oligophenyldithiols would be very good candidates to serve as collector barrier in the molecular MIMIM.

The absolute conductance value of molecular junctions with conjugated molecules is not higher than that of alkanes. Considering the possible application as wires in future molecular electronic devices, this is a disappointing observation. But the length dependence is much more like a wire although still exponential. If one could lower the contact resistance to the molecules, longer oligophenyldithiols are good candidates to serve as interconnects in molecular electronic circuits.

3.2. Emitter barrier: SiO_2

Growing silicon oxide is a very well known process from semiconductor industry. The O in the abbreviation MOS-technology (from Metal Oxide Semiconductor technology) is very often referring to SiO_2, although nowadays chipmakers are switching to Hafnium-oxide compounds in their search for high-k dielectrics for application in field-effect transistor gate dielectrics. SiO_2 layers are not only used for FETs, but also for MIS diodes. This last application is perfectly equivalent to the emitter tunneling barrier in our MIMIM transistor, except the fact that we do not need rectification. By using a heavily doped silicon wafer (10^{19}< dopants per cm^3) we diminish rectification to a reasonable level.
From experiments with tunneling diodes it is known that the oxide barrier has to be thinner than 4 nm to make any tunnel current possible.[42] Another requirement is that the oxide has to be pinhole free to avoid leakage current, which would degrade the transfer ratio of the MIMIM. It is also required that the interface between oxide and silicon is metal-contaminant free to prevent gap states. These gap states cause a larger energy spread of the injected electron beam which again degrades the transfer ratio of the transistor.

There are two ways to create a silicon oxide: chemically or thermally. To create the highest quality oxide, thermal oxidation is the best choice. Next to that it is also easier than chemical oxidation. Thermal oxidation comes in different variants: dry or wet. For wet oxidation, steam is added to the flow of oxygen which results in a faster oxidation, but less high quality oxide. This method is mostly used to create thick layers of oxide. The preferable choice for the emitter barrier is thus dry thermal oxidation. We will use heavily doped prime quality <100> wafers with 500nm pregrown SiO_2 from Silicon Quest Int. With the help of optical lithography and a buffered HF etch we define via

holes in the oxide layer with a diameter ranging from 10 to 100 µm. The so-called RCA-clean (well known from MOS industry) removes organic and metallic contaminants and after these steps a last quick HF etch removes the native oxide. Then we grow in a thermal oxidation furnace in 5 minutes at 800 °C a 2.8nm thick layer of SiO_2. We perform a post oxidation annealing step in a nitrogen flow at the same temperature as the oxidation to minimize defects in the layer and thereby increase the breakdown voltage. To be able to measure the current through the oxide we need a top electrode which is made of a 1nm layer of Cr for adhesion and a 60nm layer of Au. We have written down full experimental details in Appendix C.

In Figure 13A J-V characteristics are plotted. The scaling of the currents for different device areas is very good. The shape of the J-V plot is very similar to the J-V plot shown Dahlke and Sze[43] for a similarly prepared device. For negative bias which means tunneling from metal into the semiconductor for our setup, the device shows plain direct tunneling, judging from the shape of the J-V trace. For positive bias and above 1V the current density increases relatively to the direct tunneling curve. This extra current could be attributed to tunneling from the silicon valence band as the silicon bandgap is ~1.1V (see Figure 14 (e)). Nevertheless, Dahlke and Sze do not observe this effect for n^{++} samples. Most probably it is due to midgap states (interface states) caused by metal ions at the silicon surface (see Figure 14 (d) and (e)), which we forgot to remove for the wafer from which we show results here
In Figure 13B we show a breakdown curve of a single device. At ~3.3V we observe a sudden increase in current and after we applied this bias the device was short circuited. We have done this measurement for 10 different devices with different areas and we observed a breakdown voltage of 3.39 ± 0.218 V, which means a breakdown field of ~10MV/cm.
We also made a MIS diode in our first MIMIM wafer, but between the oxide and gold 3-mercaptopyl)trimethoxysilane replaced chromium, which could have increased the oxide by a critical amount as the currents we observed were very low (In the pA – nA range). Nevertheless the large areas of these devices showed nice symmetric J-V characteristics with a little increase in current relative to the direct tunneling curve when the positive bias was larger than 1.1V.

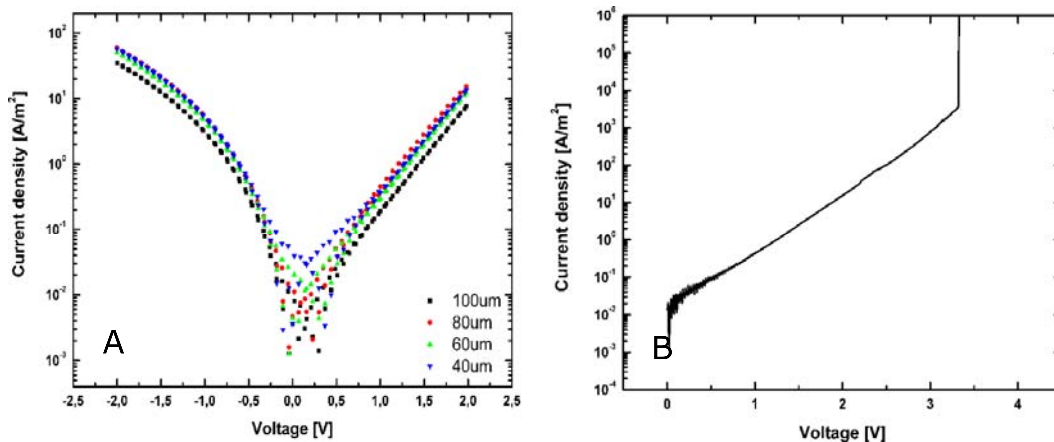

Figure 13 *(A) J-V plot of a MIS-diode with 2.8 nm SiO_2. At low biases the currents were so small that the we could not measure them properly. (B) a J-V plot of a single device that we biased over the breakdown voltage.*

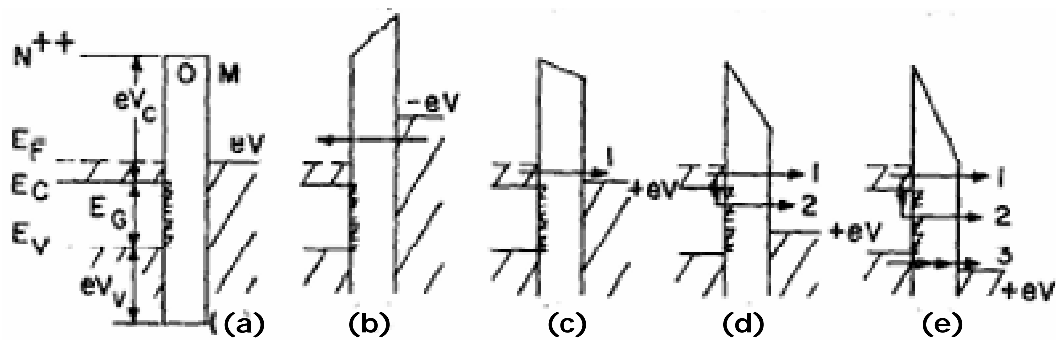

Figure 14 *Energy band diagram of a MIS diode in different bias regimes. n^{++} type silicon semiconductor layer (a) V=0, in equilibrium all surface states are filled (b) V<0, tunneling of electrons into the unoccupied conduction band (c) V>0, tunneling of electrons from conduction band into the metal. (d) V>0, tunneling of electrons from conduction band and from interface states into the metal (e) V>0, tunneling of electrons from conduction band, interface states and valence band into metal. Adapted from reference [43].*

We have made a thermally grown silicon oxide layer of decent quality that could serve as an emitter barrier. The thickness of the layer is ~2.8nm which gives reasonably high current densities, but somewhat higher currents would be better due to measurement limitations and considering the need for a much higher collector impedance than emitter impedance (requirement (a), chapter 2.3). We think the layers are also relatively pinhole free, as the breakdown field is ~10MV/cm which is pretty high for such an oxide. Makihara and coworkers[44] had to use a controlled preoxide growth process to increase the breakdown field from 1MV/cm to 10MV/cm. If we want a higher quality oxide it could still be advantageous to use a controlled pre-oxidation mechanism. Because the first layers of oxide grown determine the quality of the rest of the oxide layer (oxide grows 'into' the material). We can not say anything about the energy spread of the tunneling energy beam. To be able to do this, we need capacitance-voltage measurements to acquire more information about the gap states induced by the metal ions on the Si-SiO_2 surface. Another characterization we have to do is to measure the absolute value of the current densities as a function of oxide layer thickness. If we have this information we can compare our devices better to previous measurements.

3.3. Base layer: ultra-thin Au

The base layer has to meet several though requirements. First, the base layer of a MIMIM has to be very thin to enable electrons to traverse ballistically. How thin exactly is determined by the mean free path of the ballistic electrons. Note that the mean free path of hot electrons is different from the mean free path mentioned in connection with conductivity of metals. The electron mean free path in a metal is determined by several scattering mechanisms: electron-defect or electron-impurity, electron phonon and electron–electron collisions.[13] The basic thing to remember is that the mean free path decreases as the hot electron excess energy increases. The first thing we want to measure with the MIMIM is the barrier height of molecules in the collector junction. To determine the barrier height, ballistic electrons emitted by the emitter should be able surpass the molecular barrier. This means that the electrons should be able to traverse the base and arrive at the molecular barrier with an excess energy minimally the barrier height. So we need an estimate of this barrier height to determine the required

base thickness. An upper estimate of the barrier height would be half the optical gap. For the conjugated molecules from chapter 3.1 this would mean ~1.75 eV. According to reference [45] an excess energy of 2 eV results in a mean free path of 20nm maximally at 300°K, so our base thickness should be below 20 nm.
The second requirement for the base layer is that the roughness has to be low enough to ensure formation of a relatively defect free SAM. Normally, the roughness of the bottom electrode in a large area molecular junction is about 1 nm. Current increases five fold if the roughness increases 40%.[35] We have to note that it is not clear if this increase in current is only due to roughness or if grain size plays an important role too since both roughness and grain size increased in the experiments. We are not able to investigate the role of grain size and roughness independently. The consequence of increasing the roughness more than 40% is hard to predict.
The third requirement is opposing the first. The base layer has to be pinhole free to avoid short circuit pathways between collector and emitter. It is very difficult to make a thin layer that is pinhole free, especially if one considers the 3D-growth manner of gold.

We have several options to realize a base layer that meets all these requirements. The first try is to use our standard gold thermal evaporation techniques. The second is based on the first, but now we do not start evaporation at a slow rate, but immediately at a high rate of 1 nm s^{-1}. The last option is based on a paper recently published[46] in which the authors claim to create gold layers with a RMS roughness of 0.2 nanometer over an area of 1 μm^2. This is done by growing a (3-mercaptopropyl)trimethoxysilane (MPS) on an oxidized silicon substrate on which they e-beam evaporate 20 nm of gold. Because the thiols bind the gold, 2D growth is promoted resulting in a flatter layer. It is even not necessary anymore to add a Cr adhesion layer below the gold. We do not have an e-beam evaporator, so we use a thermal evaporator. For full experimental details we would like to refer to Appendix D.

A scanning tunneling microscope (picoLE 5100 AFM/SPM microscope, Agilent technologies) was used to characterize the Au layers. In Figure 15 we summarize the images and in Table 4 the extracted data with experimental parameters. It turns out to be not so difficult to create an ultra-thin gold layer with the desired roughness, for example when looking at Figure 15C. With an evaporation rate of 1nm s^{-1} from the beginning we made this 15 nm thick gold layer with no pinholes and a RMS roughness of 0.49 nm. The other two methods pictured in Figure 15A and Figure 15E also give layers good enough to serve as a SAM substrate without pinholes.
Despite these encouraging results, layer quality degrades after the processing steps we have to take to realize a fully functional MIMIM. On top of the base layer we photolithographically define small holes. Since the photoresist has to be hard enough to withstand 1.5 day in a SAM solution, we have to anneal the entire wafer at 200°C for at least 2 hours. Akkerman and coworkers report that the gold layer reconstructs when it is annealed.[35] For thick layers this reconstruction results in a decrease of the roughness, but it turns out that the annealing step is disadvantageous for thin layers as we show in the bottom row of Figure 15. Not only the roughness increases dramatically, but also pinholes form. The scale of the pictures after annealing is for the last two methods as large as or larger than the thickness of the layer.

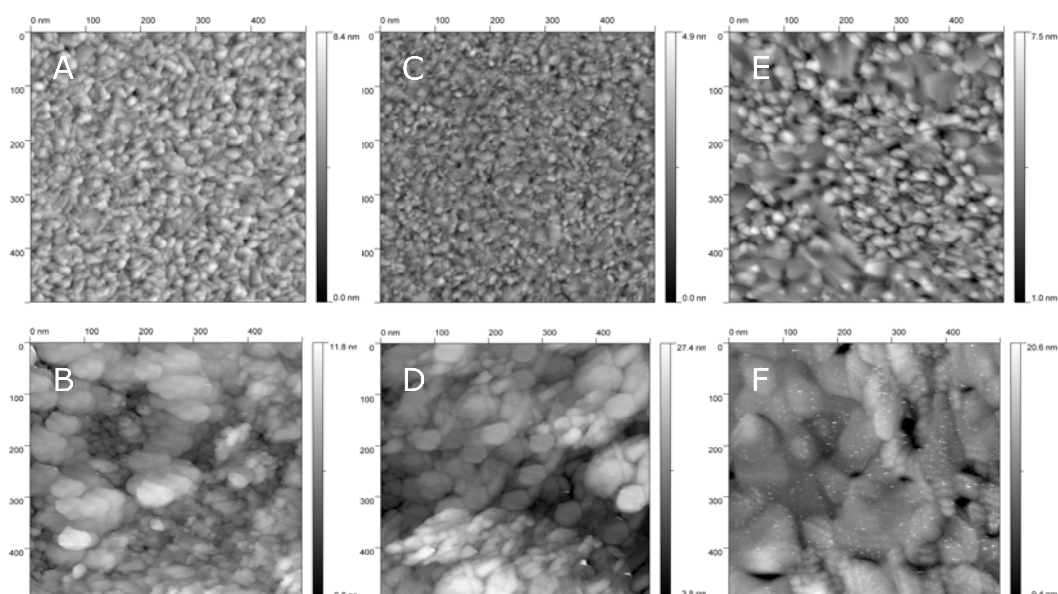

Figure 15 *Overview of the STM images of ultra-thin Au layers created with different methods. On the top row the freshly evaporated gold and on the bottom row the same layers annealed at 200 °C for a minimum of two hours. We have summarized the experimental parameters in Table 4.*

Picture	Layer thickness	Method	Roughness (0.25 μm^2 area) [nm]	Scale [nm]	Roughness after annealing	Scale after annealing [nm]
A-B	15nm(Au) 1nm (Cr)	Gradually start, Au: 0.5 nm/s	0.99	10	1.55	7
C-D	17nm(Au) 1nm(Cr)	Au: 1 nm/s	0.49	4	4,1	23
E-F	21 nm Au (MPS)	Au: 0.05nm/s	0.99	7	2.58	20

Table 4 *Overview data of different methods to create an Au base layer.*

The molecular MIMIM needs a base layer thinner than 20nm to let the electrons traverse ballistically. We have used three different methods to create an ultra-thin Au base layer. Although the freshly evaporated gold layers were all suitable for SAM formation, the annealing step degrades the quality of the layers significantly. If we look at the STM pictures we should choose the MPS-method: although there are some pinholes, the layer is reasonably flat and shows quite large domains. This method is also most susceptible for improvements as it is not clear if the MPS monolayer was closely packed for the Au layers we made. We have been investigating improvements in MPS monolayer formation, but have no clear results. Considering only roughness as the relevant parameter for SAM formation, standard gold evaporation would be the best method. The roughness of this layer is only 1.55 nm in comparison to 2.58 for the MPS layer.

Using a different metal than gold could be a radical other possibility. Since gold exhibits 3D-growth it is actually not the first choice to create ultra-thin, ultra-flat and pinhole-free layers. A new material should meet the requirements mentioned in the introduction of this paragraph, but should also be a good substrate for monolayer formation, should have a suitable work function and should be hard to oxidize.

4 MIMIM functionality

Chapter 3 was devoted to development of the separate elements of a molecular MIMIM transistor according to the requirements and considerations in paragraph 2.3. In this chapter we combine the knowledge obtained so far to realize the full device according to the processing scheme from Figure 6 in chapter 2. We will use a 2.8 nm SiO_2 layer and put a (3-mercaptopropyl) trimethoxysilane SAM on top to serve as a sticking and roughness reducing layer for the gold base layer of 20 nm thick. For the collector barrier we will use the quaterphenyldithiol, because it is the longest molecule which results in the highest collector-base resistance and it is the molecule with the lowest barrier according to Fowler-Nordheim tunneling regime measurements. Since we could not see a signature of the oligophenyldithiols for molecular junctions processed at the University of Groningen, we would like to do the experiments at PRLE, but for the MIMIM this is not possible due to wafer size and layout. But since we think the difference between PRLE and the University of Groningen is a contact barrier it is alright to do the processing in Groningen.
Two basic parameters characterize the molecular MIMIM: transfer ratio α and collector barrier height. The transfer ratio determines not only the quality of the device as an amplifier but also the preciseness of the barrier height measurement. We can easily obtain the transfer ratio by dividing collector current and emitter current. The collector barrier height determines if we can use molecules as functional elements in a MIMIM and gives us insight in the charge transport mechanisms through molecules. We can determine the collector barrier height by detecting the emitter voltage at which the collector current suddenly increases. When applying negative voltages to the emitter ballistic electrons are emitted and we could determine the position of the LUMO of the molecule. When applying positive emitter voltages ballistic holes are emitted and we could determine the HOMO of the molecule. All measurements can be done in common base setup like we showed in Figure 2 in chapter 2.

Concerning the results of the MIMIM measurements, we want to stress that due to the layout of the wafer devices of one size are all at once measured in parallel. The emitter contact (Si n^{++} wafer) is common for all devices and the collector contact (Au strip) is common for one device size (see Figure 16). There are several consequences of this layout mistake:

-We cannot measure the current of a single emitter junction. Via the collector current from the other devices is also measured.

-The same holds for the collector junction, although the parallel paths through the emitter barrier have a much higher resistance so the influence of these parasitic currents is not so large.

-We cannot really measure in a 3 terminal setup. If collector and emitter are connected a bias is applied over all devices, still we can connect the base of one device. This means most of the devices have a floating base contact. Because the emitter junction impedance is so high, almost all voltage drops over this junction. This means the shape of the collector barrier is not altered, so we are still able to measure the molecular barrier height.

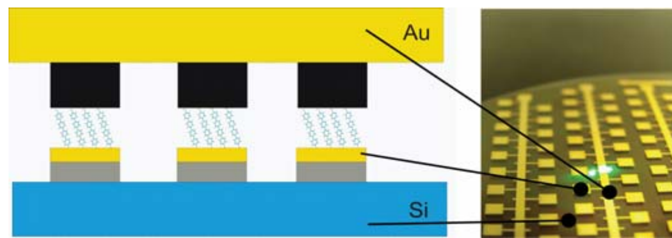

Figure 16 *Left: a schematic overview of the parallel device setup. Right: a photograph of one of our wafers. The lines show with which part of the wafer the schematically depicted contacts correspond.*

When we isolated the devices, the currents were too low to measure. All results we present here are only from a first test experiment. There are too many things that could have possibly gone wrong to call this experiment conclusive. Still, the current we measure in the emitter lead is really the current that we send through the devices and the current in the collector lead is the current that has passed the collector barrier.

Figure 17A and B show the basic results. For different base-collector biases we performed a V_{be} sweep up to 3V and up to -3V (oxide breakdown voltage was measured to be 3.39V, paragraph 3.2) and recorded the collector and emitter currents. Depending on the collector bias, we see a sudden increase of the collector current between -2.2V and -2.4V for negative emitter voltages and between 2.2V and 2.7V for positive emitter voltages. Above the onset point the collector current follows the emitter current. That means if carriers are really surmounting the barrier the transfer of hot electrons is quite good. The maximum transfer ratio $\alpha=I_c/I_e$ of the device is 0.67 at 3V and 0.83 at -3V. A severe issue of these measurements is the occurrence of hysteresis in the collector current as we show in Figure 17C. Normally this means that we damage and charge something, but when we do a second up-sweep the original curves return.
The influence of the collector bias is another big point of discussion. Although we have to take image forces into account, it is still strange that the very small collector bias voltages change the onset point so much. Collector biases are at maximum 10 μV, because leakage currents (direct tunneling) through the molecular collector barrier are very high. Figure 17D shows multiple sweeps for higher collector biases: due to the small resistance of the molecule the onset point is already obscured at V_{bc}=40μV. In Figure 17E we show a measurement with a high collector bias of 50mV. At -1.39V we still see an onset of the current with a magnitude that is similar to the emitter current. This observation is in contradiction with the claim we made in the previous sentence.
Another feature that draws attention is the sawtooth pattern in the collector current when the device is in the “off-state”. Probably these peaks occur due to charging effects of the base layer. For the measurements shown in Figure 18, these charging effects did not occur, so probably they are no artefact of the measurment apparatus.
The hysteresis observed for the measurements shown in Figure 17 is a large devaluation of the data extracted from those measurements. Therefore in Figure 18 we show characteristics of another strip of devices. In these measurements the onset point at ~2V was also visible, but the measurements were very noisy at higher emitter voltages. The emitter I-V characteristics did not scale very well either as shown in Figure 24, Appendix E. But for this device size we could see another onset point, which occurred with a relatively low amount of hysteresis. For positive emitter voltages the onset point is 1.26 ± 0.140 V and for negative emitter voltages -1.17 ± 0.067 V. Transfer ratios are very low: in the order of 10^{-6}. Due to the low transfer ratio this onset point was not visible in the measurements on the 60 μm and 100 μm devices shown in Figure 17. It was obscured by the the sawtooth collector current profile.

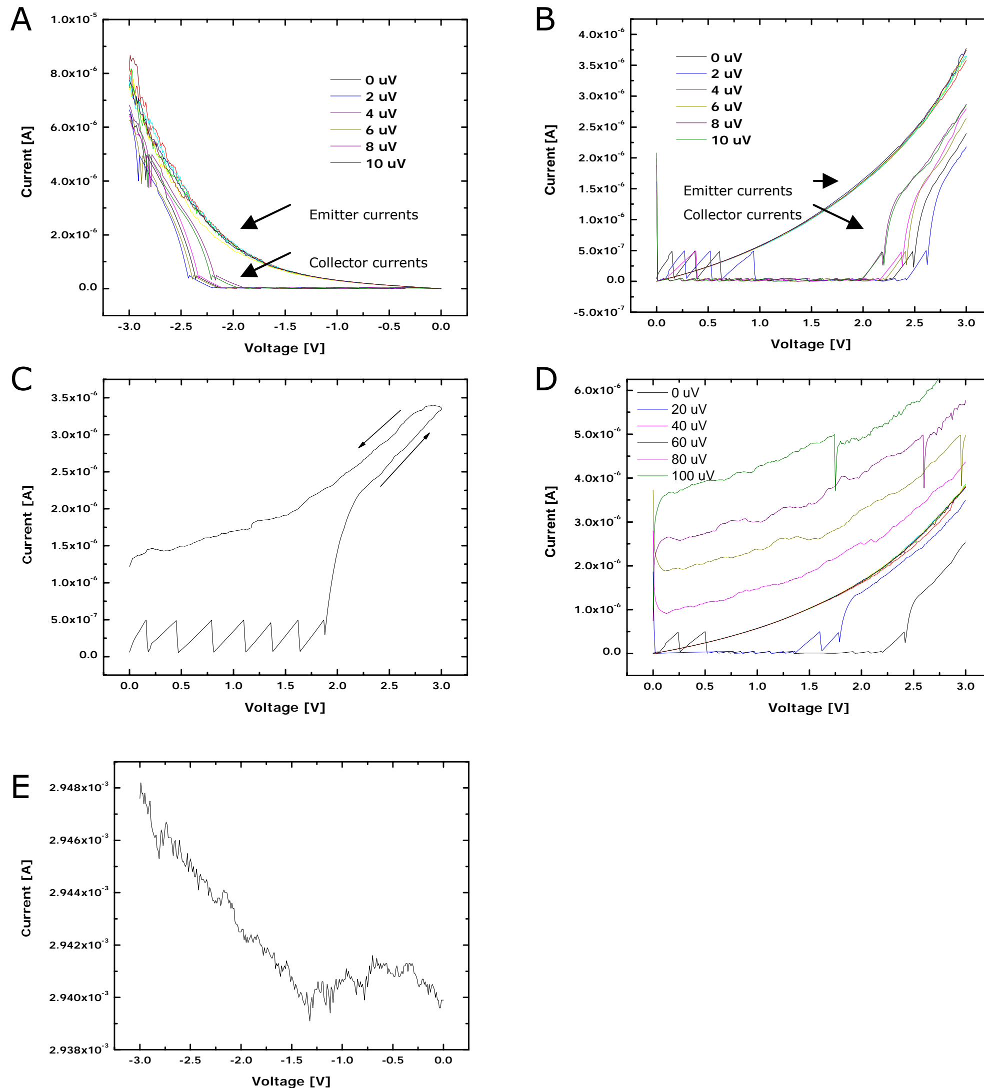

Figure 17 *Common base current measurements versus emitter voltage. Absolute values are plotted for the currents (a) 100µm devices, negative emitter voltages, different collector biases 0-10 µV. (b) 60µm devices, positive emitter voltages, different collector biases 0-10 µV. (c) 60µm devices, positive emitter voltages with different collector biases 0-100 µV.(d) 100 µm devices collector current versus emitter voltage up and down sweep. (e) 100µm, devices negative emitter, 50mV collector bias.*

Figure 18A and B are quasi 3-terminal measurements like the measurements in Figure 17. As pointed out in the introduction of this chapter, the quasi 3-terminal setup is almost similar to a two terminal setup with contacts to the emitter and collector. To show the similarity we performed these 2-terminal measurements and show the results in Figure 18C and D.

We are very reluctant to draw conclusions from the presented MIMIM measurements. The parallel device layout, hysteresis, non-scaling emitter current of the 20µm strip and an unexpected collector bias response are major issues encountered for the first MIMIM wafer we produced. Despite these problems we were able to extract collector current onset points. Two were observed and because of the lack of hysteresis we trust the lower value more than the higher.

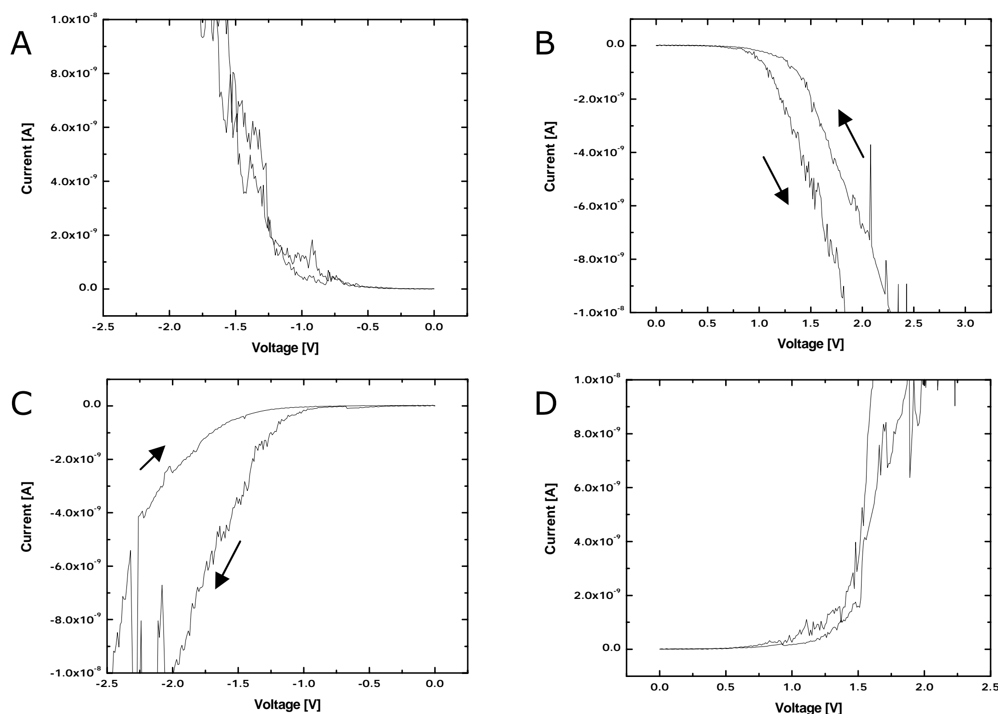

Figure 18 *Current versus voltage characteristics of 20 μm devices The arrows indicate the direction of the sweep (a) Collector current of quasi 3-terminal setup negative emitter voltages (b) Collector current of quasi 3-terminal setup positive emitter voltages (c) current through the device in 2-terminal setup negative emitter bias (d) current through the device in 2-terminal setup with positive emitter bias.*

Due to these issues we do not dare to relate the observed current onset points to molecular barriers. The values of the lower onset points are more realistic than the higher onset points if one considers the HOMO-LUMO gap of P4DT measured by de Boer and coworkers. They measure an optical gap in solution of 3.44 eV with UV-Vis spectroscopy. If the onset points correlate with the HOMO and LUMO one could calculate the gap by adding the measured positive onset point and the negative onset point. For the lower onset points this leads to a gap of 1.43 eV and for the higher onset points to 5.1 eV. These values are another argument for the lower onset point to be somehow related to the barrier height as it is unlikely that the HOMO-LUMO gap increases when a molecule is connected between two electrodes.
With the help of the measurements performed we can give recommendations for improvements of the molecular MIMIM. First of all each device needs a separate collector contact. The strip needs to be interrupted to allow each device to be measured independently. Secondly, to minimize collector leakage current, we need a high collector impedance which can be realized by taking a longer conjugated molecule for the collector barrier. After these two basic improvements have been implemented we can continue characterization and development of the rest of the layers in the molecular MIMIM. For example, at this point we can not say anything about the energy loss in the gold base layer and SiO_2 barrier. If the collector barrier would be leakage current free we could measure the energy distribution of the ballistic electron beam when it arrives at the collector barrier by deploying conventional MIMIM electron energy spectroscopy techniques (paragraph 2.5). These data give us the means to judge whether the thickness of the base layer is right and if all the electrons injected by the emitter are hot electrons.

5 Conclusion/outlook

A transistor made with self-assembled molecules could overcome the size limits in chip fabrication imposed by photolithography. A suitable device concept for this molecular transistor is the MIMIM transistor proposed by C.A. Mead in 1960. The device consists of two insulating barriers sandwiched between three metal electrodes. The idea is to make these two energy barriers with insulating molecules. Current understanding of electronic transport through molecules is to see the molecules as an energy barrier through which the electrons tunnel. If this is true, molecules would be very suitable candidates for the insulating barriers of a MIMIM, since they are very small and self-assemble in ordered monolayers.

One of the two most important requirements for a MIMIM transistor is a low and thick base-collector barrier. We tested oligophenyldithiols of three different lengths in two terminal large-area molecular junctions and concluded the quaterphenyldithiol to be most suitable as collector barrier. The RS-values of the junctions with these molecules are exponentially dependent on length with a decay constant of β=0.294 $Å^{-1}$. The barrier height of P4DT was determined to be below 1 eV by Fowler-Nordheim measurements and a Simmons model fit to the decay constant. The second important MIMIM requirement is a thin base layer. A thin base layer means less than 20 nm. This is not easily realizable with standard Au evaporation techniques. With a adhesion/planarization layer of (3-mercaptopropyl)trimethoxysilane (MPS) under the gold we could increase the quality of the layer but still not satisfying enough. Further research has to be done on this subject.

The only MIMIM transistor we realized was not suitable as a switching device because next to the fabrication problems, the collector-base junction had a too low impedance. In theory the device could still be used to determine the molecular barrier height of the collector barrier. We observed onset points in two different ranges, one around 2 Volts and one at 1.26 and -1.17 Volts. The lower values are most trustworthy, but we are very reluctant to relate these values to the energy barriers the molecule induces. If we solve the issues with the SiO_2 emitter barrier MIMIM transistor we have a very powerful tool to fundamentally study the transport through single molecules. The large-area molecular junction is a versatile testbed that can incorporate all self assembling molecules. This means that we can probe the energy level dependent transport of all these molecules directly.

The ultimate goal of this research is a fully molecular MIMIM transistor that could replace silicon transistors. The first progress towards this objective has been made. Still, there are a lot of problems to tackle. First we need a collector barrier with a high impedance, which means we need to use a longer conjugated molecule. Secondly we have to make an emitter barrier from molecules, which is an enormous technical challenge, because of the special requirements of the base layer and the vulnerability of the molecules. One of the possible routes is to create a base layer with the nanotransfer printing technique. The disadvantage of this method is that we have to develop and characterize a totally new contact technique. The most promising way is to process two large-area molecular junctions on the same bottom contact layer. This means finding a way to reach the bottom of the bottom contact layer of the first junction, which will be very difficult. The advantage of this method is that the contacts to the molecules are the same as in large-area molecular junctions so contact characterization can be skipped.

6 Acknowledgements

First of all I would like to thank my professors Paul Blom and Bert de Boer for enabling me to do my master research in their group, but also for the useful early Monday morning workmeetings and the freedom they gave me to conduct my research. An extra word of thanks is for Bert de Boer since he helped me a lot with my Toptalent proposal and he wrote quite some very nice recommendation letters and emails for me.
I am very grateful to have worked under direct supervision of Auke J. Kronemeijer and Hylke B. Akkerman. As the master of large-area molecular junctions Hylke had always already done the 'genious' experiment you came up with. Auke was my direct supervisor and I would like to thank him very much for his close assistance and many useful discussions. He even drove me to Eindhoven to enable me to make the conjugated molecules work. I would also like to show my special appreciation to the other molecular electronics guys Eek Huisman and Ilias Katsouras. The useful discussions and other interhuman contacts made my thesis year a lot nicer and educative. I cannot forget to thank Jan Harkema and Frans van der Horst for keeping the technical facilities in the ME-POS group always in top condition.
For my experiments I needed to use facilities and discussed with people throughout the faculty. When I needed a glovebox to grow SAMs in an inert environment, Ebe Schudde from professor Feringa's group helped me out with lending me a glovebox and assisting me to make it work again. Siemon Bakker helped me a lot with growing thermal oxide and setting up the first experiments in the Nanolab Groningen. Also Johan Holstein assisted me in this new facility. With Tatiana Fernández Landaluce I had some very useful discussions on growing silanes.
At Philips Research Laboratories Eindhoven are also quite some people I would like to thank. First of all Paul van Hal, who co-developed the procedure to grow inert SAMs at PRLE and took me by the hand while doing the processing. Ton Geuns made all the very nice wafers for us. Ton van den Biggelaar lended us his glovebox and Johan Klootwijk gave some tips for growing thermal silicon oxide.
And last but not least I am very grateful to have been part of the ME-POS group for an entire year. Working in the clean room, chatting during breaks, partying in Hasselt and monday morning workmeetings have all been part of a wonderful experience. I would like to thank the group very much for the wonderful time!

7 Bibliography

1. Mead, C. The tunnel emission amplifier. *Proceeedings of the IRE* **48**, 359-361(1960).
2. Lacour, D. et al. Hot-electron transport in 3-terminal devices based on magnetic tunnel junctions. *EPL (Europhysics Letters)* **60**, 896-902(2002).
3. Saitoh, W. et al. Metal (CoSi 2)/Insulator (CaF 2) Hot Electron Transistor Fabricated by Electron-Beam Lithography on a Si Substrate. *Jpn. J. Appl. Phys.* **34**, L1254-L1256(1995).
4. Akkerman, H.B. et al. Towards molecular electronics with large-area molecular junctions. *Nature* **441**, 69-72(2006).
5. Kushmerick, J. et al. Vibronic Contributions to Charge Transport Across Molecular Junctions. *Nano Lett.* **4**, 639-642(2004).
6. Jun, Y. & Zhu, X. FTIR Spectroscopy of Buried Interfaces in Molecular Junctions. *J. Am. Chem. Soc.* **126**, 13224-13225(2004).
7. A. Salomon, T.B. What is the Barrier for Tunneling Through Alkyl Monolayers? Results from n- and p-Si-Alkyl/Hg Junctions. *Advanced Materials* **19**, 445-450(2007).
8. Akkerman, H.B. et al. Electron tunneling through alkanedithiol self-assembled monolayers in large-area molecular junctions. *Proceedings of the National Academy of Sciences* **104**, 11161-11166(2007).
9. Beebe, J.M. et al. Transition from Direct Tunneling to Field Emission in Metal-Molecule-Metal Junctions. *Phys. Rev. Lett.* **97**, 026801-4(2006).
10. Quinn, J. et al. Oxidation Potentials Correlate with Conductivities of Aromatic Molecular Wires. *J. Am. Chem. Soc.* **129**, 12376-12377(2007).
11. Li, W. et al. Ballistic Electron Emission Microscopy Studies of Au/Molecule/n-GaAs Diodes. *J. Phys. Chem. B* **109**, 6252-6256(2005).
12. Goossens, A. Tunneling hot carrier transistors. *not published* (2007).
13. Heiblum, M. Tunneling hot electron transfer amplifiers (theta): Amplifiers operating up to the infrared. *Solid-State Electronics* **24**, 343-366(1981).
14. Luryi, S. & Kastalsky, A. Hot-electron transport in heterostructure devices. *Physica B+C* **134**, 453-465(1985).
15. Mead, C.A. Operation of Tunnel-Emission Devices. *J. Appl. Phys.* **32**, 646-652(1961).
16. Nelson, O.L. & Anderson, D.E. Hot-Electron Transfer through Thin-Film Al[Single Bond]Al[sub 2]O[sub 3] Triodes. *J. Appl. Phys.* **37**, 66-76(1966).
17. Huber, J., Johnston, J. & Kirk, J. Hot-Electron Transport in Al[Single Bond]Al[sub 2]O[sub 3] Triodes Produced by Plasma Oxidation. *J. Appl. Phys.* **39**, 5104-5116(1968).
18. Antula, J. Experimental Evidence of Hot-Electron Transport through Thin Metal Films. *J. Appl. Phys.* **43**, 1830-1834(1972).
19. Antula, J. A method of investigation of hot electron transport through thin metal films using the metal-base triode configuration*1. *Thin Solid Films* **13**, 93-97(1972).
20. Chao, Y. et al. Polymer hot-carrier transistor. *Appl. Phys. Lett.* **87**, 253508-3(2005).
21. Loo, Y. et al. Electrical Contacts to Molecular Layers by Nanotransfer Printing. *Nano Lett.* **3**, 913-917(2003).
22. Love, J.C. et al. Self-Assembled Monolayers of Thiolates on Metals as a Form of Nanotechnology. *Chem. Rev* **105**, 1103-1170(2005).
23. Heiblum, M. & Fischetti, M. Ballistic hot electron transistors. *IBM J. Res. Dev.* **34**, 530-549(1990).

24. Hesto, P., Pone, J. & Castagne, R. A proposal and numerical simulation of N[sup +]NN[sup +] Schottky device for ballistic and quasiballistic electron spectroscopy. *Appl. Phys. Lett.* **40**, 405-406(1982).
25. Aviram, A. & Ratner, M.A. Molecular rectifiers. *Chemical Physics Letters* **29**, 277-283(1974).
26. Kronemeijer, A.J. et al. Reversible Conductance Switching in Molecular Devices. *Advanced Materials* **20**, 1467-1473(2008).
27. Ho Choi, S., Kim, B. & Frisbie, C.D. Electrical Resistance of Long Conjugated Molecular Wires. *Science* **320**, 1482-1486(2008).
28. de Boer, B. et al. Synthesis and Characterization of Conjugated Mono- and Dithiol Oligomers and Characterization of Their Self-Assembled Monolayers. *Langmuir* **19**, 4272-4284(2003).
29. Simmons, J.G. Electric Tunnel Effect between Dissimilar Electrodes Separated by a Thin Insulating Film. *J. Appl. Phys.* **34**, 2581-2590(1963).
30. Simmons, J.G. Generalized Thermal J-V Characteristic for the Electric Tunnel Effect. *J. Appl. Phys.* **35**, 2655-2658(1964).
31. Gadzuk, J.W. & National Bureau of Standards, Washington, D. C. 20234, J. Field Emission Energy Distribution (FEED). *Reviews of Modern Physics* **45**, 487
32. Joachim, C. & Magoga, M. The effective mass of an electron when tunneling through a molecular wire. *Chemical Physics* **281**, 347-352(2002).
33. Tour, J.M. et al. Self-Assembled Monolayers and Multilayers of Conjugated Thiols, .alpha.,.omega.-Dithiols, and Thioacetyl-Containing Adsorbates. Understanding Attachments between Potential Molecular Wires and Gold Surfaces. *J. Am. Chem. Soc* **117**, 9529-9534(1995).
34. Akkerman, H.B. Large-area molecular junctions. (2008).
35. Akkerman , H.B. et al. Influence of bottom electrode roughness on the conduction through 1,12-dodecanedithiol self-assembled monolayers. *Applied Physics Letters* **Submitted**,
36. Wold, D. et al. Distance Dependence of Electron Tunneling through Self-Assembled Monolayers Measured by Conducting Probe Atomic Force Microscopy: Unsaturated versus Saturated Molecular Junctions. *J. Phys. Chem. B* **106**, 2813-2816(2002).
37. Holmlin, R. et al. Electron Transport through Thin Organic Films in Metal-Insulator-Metal Junctions Based on Self-Assembled Monolayers. *J. Am. Chem. Soc.* **123**, 5075-5085(2001).
38. Sachs, S. et al. Rates of Interfacial Electron Transfer through π-Conjugated Spacers. *J. Am. Chem. Soc.* **119**, 10563-10564(1997).
39. Creager, S. et al. Electron Transfer at Electrodes through Conjugated "Molecular Wire" Bridges. *J. Am. Chem. Soc.* **121**, 1059-1064(1999).
40. Kondo, M., Tada, T. & Yoshizawa, K. Wire-Length Dependence of the Conductance of Oligo(p-phenylene) Dithiolate Wires: A Consideration from Molecular Orbitals. *J. Phys. Chem. A* **108**, 9143-9149(2004).
41. Beebe, J. et al. Measuring relative barrier heights in molecular electronic junctions with transition voltage spectroscopy. *ACS Nano* **XX**, 000-000
42. Sze, S.M. *Physics of Semiconductor Devices*. 880(Wiley-Interscience: 1981).
43. Dahlke, W.E. & Sze, S.M. Tunneling in metal-oxide-silicon structures. *Solid-State Electronics* **10**, 865-873(1967).
44. Makihara, K. et al. Preoxide-Controlled Oxidation for Very Thin Oxide Films. *Jpn. J. Appl. Phys.* **32**, 294-297(1993).
45. Sze, S.M., Moll, J.L. & Sugano, T. Range-energy relation of hot electrons in gold. *Solid-State Electronics* **7**, 509-523(1964).
46. Mahapatro, A.K. et al. Gold surface with sub-nm roughness realized by evaporation on a molecular adhesion monolayer. *Appl. Phys. Lett.* **88**, 151917-3(2006).
47. Brower, T. et al. Self-Assembled Multilayers of 4,4'-Dimercaptobiphenyl Formed by Cu(II)-Catalyzed Oxidation. *Langmuir* **18**, 6207-6216(2002).
48. Azzam, W. et al. Bonding and Orientation in Self-Assembled Monolayers of Oligophenyldithiols on Au Substrates. *Langmuir* **18**, 7766-7769(2002).
49. Tao, Y. et al. Structure Evolution of Aromatic-Derivatized Thiol Monolayers on Evaporated Gold. *Langmuir* **13**, 4018-4023(1997).
50. Frey, S. et al. Structure of Thioaromatic Self-Assembled Monolayers on Gold and Silver. *Langmuir* **17**, 2408-2415(2001).

51. Krapchetov, D. et al. Solvent-Dependent Assembly of Terphenyl- and Quaterphenyldithiol on Gold and Gallium Arsenide. *Langmuir* **21**, 5887-5893(2005).
52. Fuxen, C. et al. Structural Characterization of Organothiolate Adlayers on Gold: The Case of Rigid, Aromatic Backbones. *Langmuir* **17**, 3689-3695(2001).
53. Ishida, T. et al. Adsorption Processes of Self-Assembled Monolayers Made from Terphenyl Thiols. *Langmuir* **17**, 7459-7463(2001).
54. Himmel, H., Terfort, A. & Woll, C. Fabrication of a Carboxyl-Terminated Organic Surface with Self-Assembly of Functionalized Terphenylthiols: The Importance of Hydrogen Bond Formation. *J. Am. Chem. Soc.* **120**, 12069-12074(1998).
55. Timpanaro, S. et al. Morphology and conductivity of PEDOT/PSS films studied by scanning-tunneling microscopy. *Chemical Physics Letters* **394**, 339-343(2004).

8 Appendices

Appendix A : Large Area Molecular Junction processing

The process flowchart for the fabrication of large-area molecular junctions can be subdivided in three main research focus areas, which are summarized as follows:

1. The bottom electrode.

A 4-inch silicon wafer with 500 nm thermally grown oxide is passivated using hexamethyl disilazane (HMDS) for a better adhesion of the spincoated photoresist. An adhesion layer of 1 nm Cr and the Au bottom electrodes are thermally evaporated. Subsequently, negative photoresist is spincoated on the wafer, resulting in a layer thickness of ~ 570 nm. A pre-bake step at 95 ºC on a hotplate eliminates the remaining solvents in the layer. Lithography is done with a Karl Süss MA1006 maskaligner. Vertical interconnects (or vias) are created by photolithography on top of the bottom Au electrodes, with a diameter ranging from 10–100 μm. After fabricating the vertical interconnects, the photoresist is annealed for at least 1 hour at 200 ºC in vacuum to make the photoresist insoluble in ethanol

2. The self-assembled monolayer

After plasma cleaning the bottom electrodes inside the vertical interconnects, the complete wafer is submersed for a minimum of 36 hrs in the solution of the self-assembling molecules in ethanol. The synthesis of the molecules is done according to previously published procedure[4]. The concentration of the molecules in ethanol is 3 mM. After the self-assembly of the alkanedithiolate on the Au bottom electrode, the wafer is thoroughly rinsed with ethanol, toluene and *iso*-propanol to remove the remaining (physisorbed) alkanedithiol molecules.

3. The top electrode.

Subsequently, the water-based suspension of PEDOT:PSS is spin coated. For this work, the commercially available Baytron® P HC V4 (H.C. Starck GmbH & Co.) was used with a conduction of ~ 20 S/cm. To decrease the surface tension of the PEDOT:PSS and improve the wetting on the SAM in the vertical interconnects, the non-ionic fluorosurfactant Zonyl® FSO-100 (DuPont) is added. Immediately after spincoating, the PEDOT:PSS layer is dried in a vacuum chamber. Next a 150 nm Au top electrode is thermally evaporated on top of the PEDOT:PSS layer. The Au top electrode ensures a better contact with the probes when devices are measured in a probe station under vacuum, but also serves as an etching mask in the final processing step. Reactive ion etching with O_2 is used to remove the redundant PEDOT:PSS to prevent any parasitic currents from top to bottom electrode.

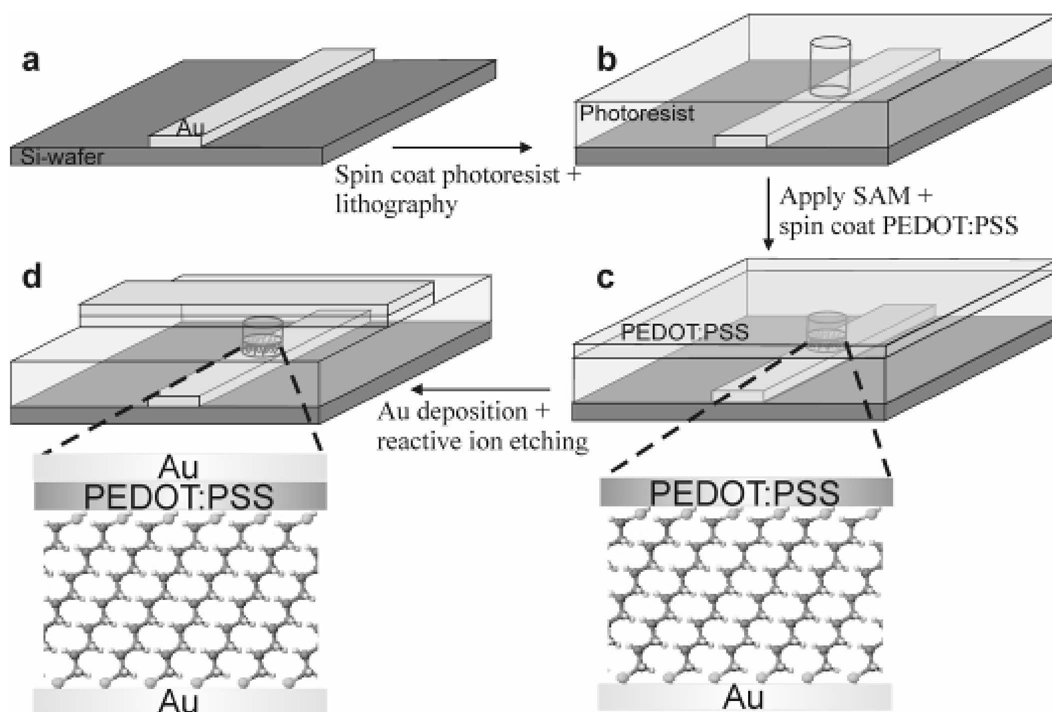

Figure 19 *Schematic overview of the processing scheme of a large-area molecular junction.*[4]

Appendix B : Oligophenyldithiol SAM formation

Oligophenyldithiol SAMs have to be processed in an inert environment to prevent polymerization of the molecules.

1. Flush the glovebox to reach an acceptable amount of oxygen (<10 ppm)

2. Weigh the molecules to get the desired concentration

3. Make sure the following equipment is in the glovebox:

   -Tweezers
   -Hotplate with stirrer
   -Stirring bar
   -Magnet for the stirring bar
   -25ml measurement cylinder
   -Funnel for the cylinder
   -Syringe and needle for Ammonia.
   -Teflon SAM formation container
   -3 Petri dishes
   -Bottle for waste solvents
   -Gloves to protect over the glovebox gloves from aggressive solvents
   -Tissues
   -Sureseal THF (tin opener for opening the sureseal bottle)
   -NH_4OH
   -Toluene
   -2-Propanol

4. Take the molecules and necessary equipment into the glovebox (flush 5 times when using the old glovebox in building 14).

5. Measure the amount of THF you need and pour it in the bottle with the molecules.

6. Set the hotplate to 75 degrees and stir for an hour. Turn the hotplate off and stir for another half hour.

7. Pour the solution in the Teflon container and add 2 drops of NH_4OH. Put the container on the stirrer to mix the NH_4OH. (only for acetyl protected molecules)

8. Put the wafer in the solution and close the Teflon container. Also close the valve of the container.

9. Wait for at least 36 hours, but not too long to prevent degradation of the photoresist by the THF.

10. Take the wafer out of the Teflon container and rinse it in Petri dishes with THF and toluene.

11. Clean the Teflon SAM container with clean THF.

12. Fill the Teflon SAM container with 2-propanol and put in the wafer. Close it again and take it out of the glovebox together with all the equipment that has to be cleaned.

13. Now you can process the wafer further according to standard Large-Area Molecular Junction procedures.

Molecule	Solvent	Concentration	Length (Å, measured)	Method	Refractive index	Tilt Angle (measured)	Method	Ref.
BPDT	Ethanol	1 uM	14.03 +/- ?	SW Ellipsometry	1.462			47
BPDT	Ethanol	1 uM	10.1 +/- 0.22	AFM (Hole digging)	-	25.6 +/- 15	AFM (Hole digging)	47
BPDT	Ethanol	1 uM	10.4 +/- 0.18	AFM (nanografting)	-	21.8 +/- 13	AFM (nanografting)	47
BPDT	Chloroform	100 uM	16.5 +/- 1.25	XPS				48
BPDT	THF	1mM	15.1 (1d) 17.3(3d)	SW Ellipsometry	-	-	-	33
BPDTAc	THF (NH4OH)	5uM	9.7+/- 1.1	SW Ellipsometry	1.55	-	-	28
BPDTAc	THF	0.5 mM	7.8 (1d)	SW Ellipsometry	-	-	-	33
BPDTAc	THF	31mM	20.5 (1d)	SW Ellipsometry	-	-	-	33
BPDTAc	THF (NH4OH)	0.5 mM	15.0 (1d)	SW Ellipsometry	-	-	-	33
BPT	THF/Ethanol	0.25 mM	9.4 +/- ?	SW Ellipsometry	1.47	-	-	49
BPT	Ethanol	5 mM	11.00 +/- 0.3	NEXAFS	-	23 +/- 5	NEXAFS	50
BPT	Ethanol	5 mM	11.54 +/- 0.7	XPS	-	23 +/- 5	NEXAFS	50
BPT	Chloroform	100 uM	12 +/- 1	XPS				48
BPT	THF	1 mM	4.9 (1h) 10.2(1d)	SW Ellipsometry	-	-	-	33
BPTAc	THF	1mM	6.6 (1h) 6.9 (1d)	SW Ellipsometry	-	-	-	33
BPTAc	THF	38 mM	8.9 (1d)	SW Ellipsometry	-	-	-	33
BPTAc	THF (NH4OH)	1 mM	10.6 (1d)	SW Ellipsometry	-	-	-	33
TPDT	THF/Ethanol (NH4OH)	50 uM	17 +/- 1	Spectrometric Ellipsometry	1.55	32 +/- 3 (solvent dep.)	NEXAFS	51
TPDTAc	THF (NH4OH)	50uM	13.7 +/- 1.9	SW Ellipsometry	1.55	-	-	28
TPT	Ethanol	5 mM	14.94 +/- 0.3	NEXAFS	-	22 +/- 5	NEXAFS	50
TPT	Ethanol	5 mM	15.25 +/- 0.7	XPS	-	22 +/- 5	NEXAFS	50
TPT	Ethanol	10 uM	21.7 +/- ?	XPS	-	~28	NEXAFS	52
TPT	Ethanol / Methylene Chloride	100 uM	-	-	-	-	-	53
TPT	Ethanol/THF	100 uM	16 +/- 1.5	XPS	-	27 +/- 5	NEXAFS	54
TPT	THF (NH4OH)	50uM	17.9 +/- 1.3	SW Ellipsometry	1.55	-	-	28
QPDT	THF/Ethanol (NH4OH)	50 uM	23 +/- 2	Spectrometric Ellipsometry	1.55	32 +/- 3 (solvent dep.)	NEXAFS	51
QPDTAc	THF (NH4OH)	10uM	22.1+/-1.3	SW Ellipsometry	1.55	-	-	28

Table 5 *Literature data on conjugated self-assembled monolayers. All monolayers assembled on Au substrates.*

Appendix C : Thermal oxidation of silicon

1. Take n++ Si wafer (SQI, 500nm oxide, R <0.005 Ω/cm, <100>, prime quality).

2. Rinse with 2-propanol, apply HMDS (without HMDS the photoresist layer detaches after the HF etch) and rinse again with 2-propanol.

3. Spincoat positive photoresist S1813 (4 ml, 5s 500 rpm, 30s 5000 rpm, we do not know the resulting layer thickness, between 0.5 and 1 μm) and prebake for 60s at 115 °C

4. Expose for 30s with positive ME mask with the custom made covering paper to prevent shorts caused by the gold evaporation mask.

5. Develop for 40s in MF-321 developer, rinse in 18.2 MΩ and spin dry.

6. Etch away the oxide with buffered HF solution (takes about 7 minutes with fresh 87.5% HF 12.5% HNO_3). Rinse wafer in demi-water.

7. Clean in H_2O:H_2SO_4:H_2O_2 5:1:1 piranha solution, 10 minutes at 60°C and rinse in demi-water

8. Clean in H_2O:HCl:H_2O_2 5:1:1, 10minutes at 60°C and rinse in demiwater cascade

9. Remove native oxide by putting wafer for 30s in 1% HF solution, rinse in demi-water cascade and spin dry

10. Immediately perform dry thermal oxidation in HiTech 1250 furnace (single horizontal tube, maximum temperature 1250 °C), according to the following heating procedure. At time=0 the wafer has entered the oven already, the oven automatically does this very slowly. The wafer has to be in between two covering wafers to create a uniform flow of oxygen at the surface of the wafer.

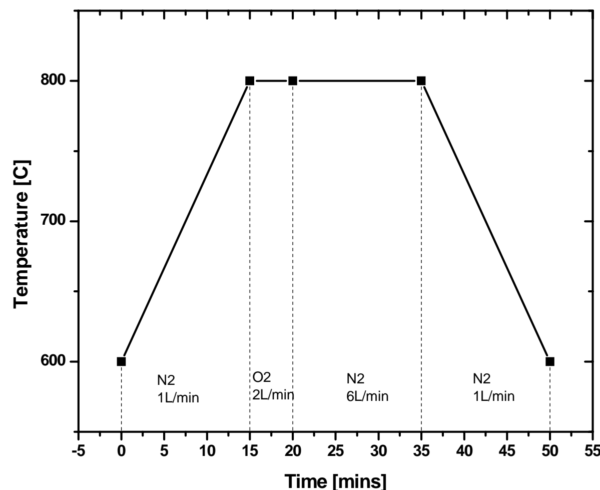

Figure 20 *Temperature profile of the oxidation procedure used. With this procedure we get around 2.8 nm of SiO_2, checked with ellipsometry.*

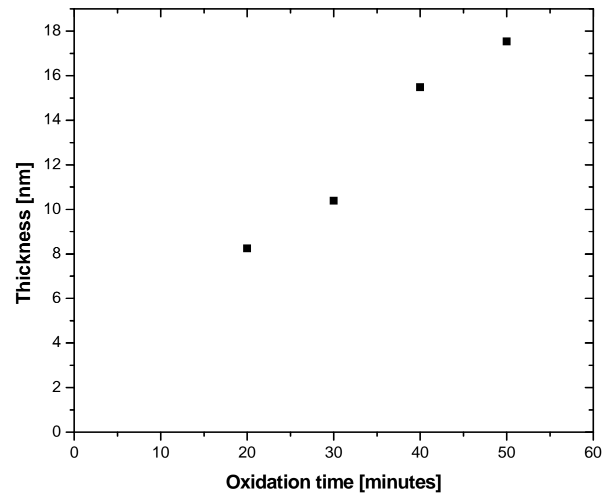

Figure 21 *Thickness in nanometer as function of the oxidation time in minutes at a temperature of 850 °C. The oxidation went too quick at this temperature so we decided to do the oxidation at 800 °C*

Appendix D : Thin Au layer formation

Method 1:
The first method used to create a thin Au layer is standard thermal evaporation of gold. First a 1 nm Cr adhesion layer is evaporated at ~0.01 nm/s. Then Au is evaporated with a slow initial evaporation rate, which is gradually increasing to 0.5 nm/s. The program used on the thermal evaporator of the ME-POS group is 25-7.

Method 2:
The second method omits the slow initial evaporation rate of the previous method and uses a faster rate from the beginning. First a 1 nm Cr adhesion layer is evaporated at ~0.01 nm/s. Then Au is evaporated at a rate of 1 nm/s.

Method 3:
This method is based on the paper by Mahapatro and coworkers[46]. With a (3-mercaptopropyl) trimethoxysilane the researchers were able to create a gold layer with a roughness of 0.2 nm over a 1 μm^2 area. In general it is not easy to make a silane SAM. There many processing parameters and they have to be optimized for each molecule. But as we only need an adhesion layer it is maybe not required to create a perfect SAM. What we basically need to do is to make the SiO_2 suitable for SAM formation. First of all we clean the oxide layer, then we expose the oxygen by putting the wafer in a UV-ozone furnace and finally we hydroxylate the exposed oxygens. For the first experiment we followed the paper as close as possible:

1. Put wafer (test quality) in a 4:1:1 H_2O:NH_4OH:H_2O_2 piranha solution at 55°C for 10 minutes to remove organic dirt and rinse in 18.2 MΩ water cascade.
2. Sonicator for 5 minutes to remove contaminations from Piranha and spin dry
3. UV-ozone for 20 minutes to expose the oxygen to the surface
4. 6:1:1 H_2O:HCl:H_2O_2 piranha at 55 °C for 10 minutes to hydroxylate the oxygen, rinse in 18.2 MΩ water and spin dry.
5. Put the wafer in the SAM solution (1mM of MPS in ethanol) and leave it for at least 1.5 days.
6. Rinse with ethanol, toluene and 2-propanol and spin dry.
7. Evaporate Au at 0.05 nm/s.

Figure 22A is the result of this experiment. Although some gold terraces are visible, the roughness is with 1 nm much higher than the claimed 0.2 nm. Some experimental details were not the same as in the paper, of which the method of SAM formation was presumably the most important. In the article the MPS SAM was formed from gas-phase, so we also tried to form the SAM in a dessicator that was evacuated for ~24 hours. Figure 22B shows the result of this experiment. All other details were the same as for the first experiment. Unfortunately the deposited layer was 50 nm thick in stead of the desired 20 nm, so we can not really say if gas phase SAM formation is an improvement. Note that both layers did not show any visible degradation after a night in THF, but that they did not withstand the scotch tape test.
We form the MPS SAM in our MIMIM on home-grown thermal SiO_2. Before growing the oxide we have already cleaned the substrate with a NH_4OH piranha and an HCl piranha. This means that when we have done the MPS-SAM preparation steps a total of 4 piranha etches have attacked the wafer, which is not advantageous for the roughness. Therefore we propose to omit the piranha steps and just put the wafer for a very long time in the UV-ozone (preferably overnight) after thermal oxidation. After the UV-ozone the wafer has to be dipped in demi-water (or 18.2 MΩ water), which is a quick hydroxylation of the exposed oxygens, and then the wafer has to be put

immediately in the SAM solution. In the first MIMIM created we used the following steps to create the Au base layer. Unfortunately we have no STM data of this layer.

1. UV-ozone for 2 hours to expose the oxygen to the surface
2. Dip the wafer in 18.2 MΩ water and spin dry.
3. Put the wafer in the SAM solution (1mM of MPS in 50% ethanol / 50% toluene) and leave it for at least 1.5 days.
4. Rinse with ethanol, toluene and 2-propanol and spin dry.
5. Evaporate Au at 0.05 nm/s.

.

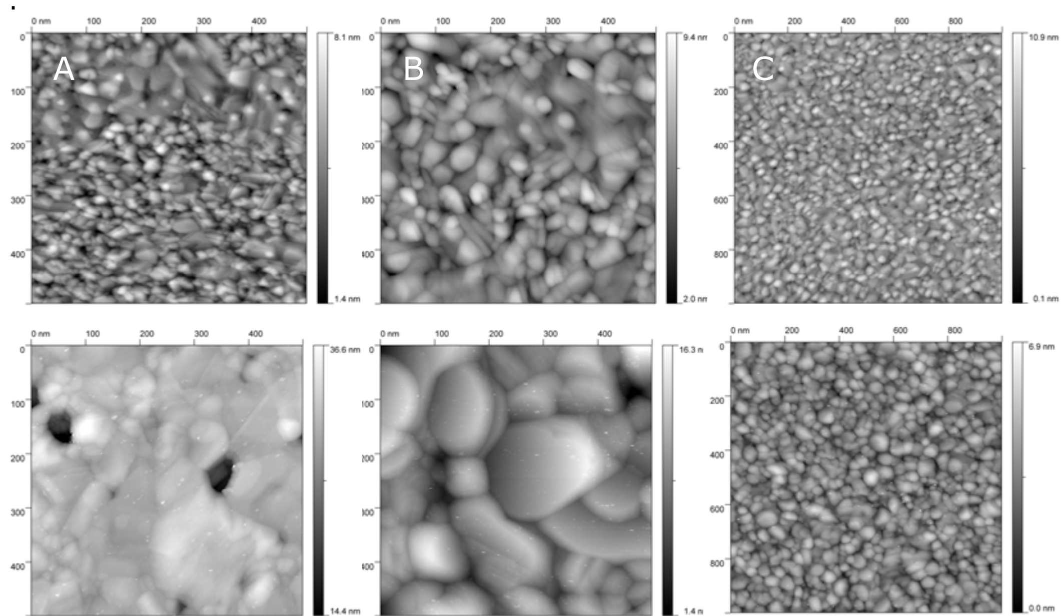

Figure 22 *Overview of STM images of Au layers before (top row) and after annealing (bottom row). (A) 20nm Au on MPS SAM formed from solution (0.25 μm^2) (B) 48nm Au on MPS SAM formed from gas phase (0.25 μm^2) RMS Roughness before annealing is 0.97 nm and after annealing 2.73 nm (C) 60nm on 1nm Cr (1 μm^2). On top the freshly evaporated surfaces and on the bottom the surfaces after annealing at 200°C for at least 2 hours. Note that for all layers the grain size increases after annealing, but for Au on MPS much more. For sample (B) the grains grow from 45.7nm to 125nm (extracted by 2D PSD analysis).*

Appendix E : MIMIM Processing

Processing a MIMIM is essentially combining the process described in Appendix A, Appendix B, Appendix C and Appendix D. First of all we have to create an emitter junction with a silicon oxide which we described in Appendix C. On top of this emitter junction we process a conventional large area molecular junction with a quaterphenyldithiol SAM which we describe in Appendix B. In Appendix B we describe how to make this SAM. The difficult step is to align the holes for the oxide vias and the holes for the SAM vias. With the markers on the side of both the negative and positive mask we can align the wafer quite well as we show in Figure 23. For very high transfer ratios we have to devise a more sophisticated method, but if we only use the larger device areas the current approach serves well enough for test purposes.
For convenience we have very briefly summarized the steps to create a MIMIM:

1. Create a silicon oxide barrier with thermal oxidation with the steps we describe in Appendix C using the positive ME lithography mask with the custom created paper mask to cover the contact pad squares.

2. Make a very thin base layer using the methods from Appendix D using the normal large-area molecular junction bottom contact evaporation mask.

3. On top of the emitter junction create a standard large area molecular junction as we describe in Appendix A with a conjugated molecule monolayer according to Appendix B. The vias of the molecular junction have to be aligned with the holes in which the SiO_2 is created, which can be done reasonably with the rectangular markers on the sides of the lithography mask. Finish the junctions with a standard top contact evaporation mask. This is not ideal as it connects all devices of one area in parallel.

4. Scratch through the photoresist layer and silicon dioxide layer and apply some silver paste to create a contact with the silicon emitter contact. Also apply silver paste to the base contacts as it is very hard to make contact to the 20nm Au layer.

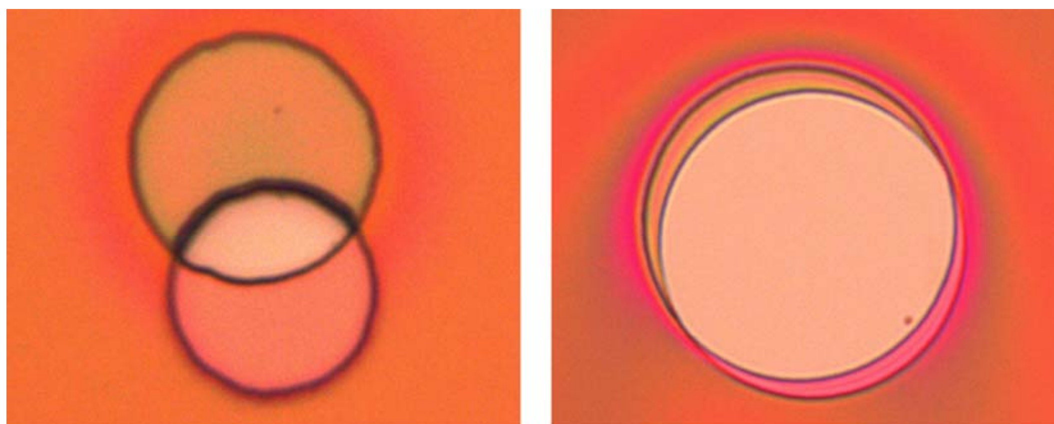

Figure 23 *Optical microscope images of 10 um (left) device and 100 um device (right)*

To see if both emitter and collector junction work well, we can characterize them independently by measuring current from base to emitter contact or from base to collector contact. In Figure 24 we have summarized the data of these measurements. These devices were measured in parallel, so current densities say not much, but at least they are reasonably low for a 2.8 nm SiO_2 emitter barrier. Although the 20 μm

devices are connected in parallel the currents are not the same. This is very strange and we do not have a good explanation for this observation.
Concerning the P4DT collector junction, the RS value is very low again, almost at the PEDOT:PSS value but comparable to previous measurements (see also Chapter 3.1, Figure 10).

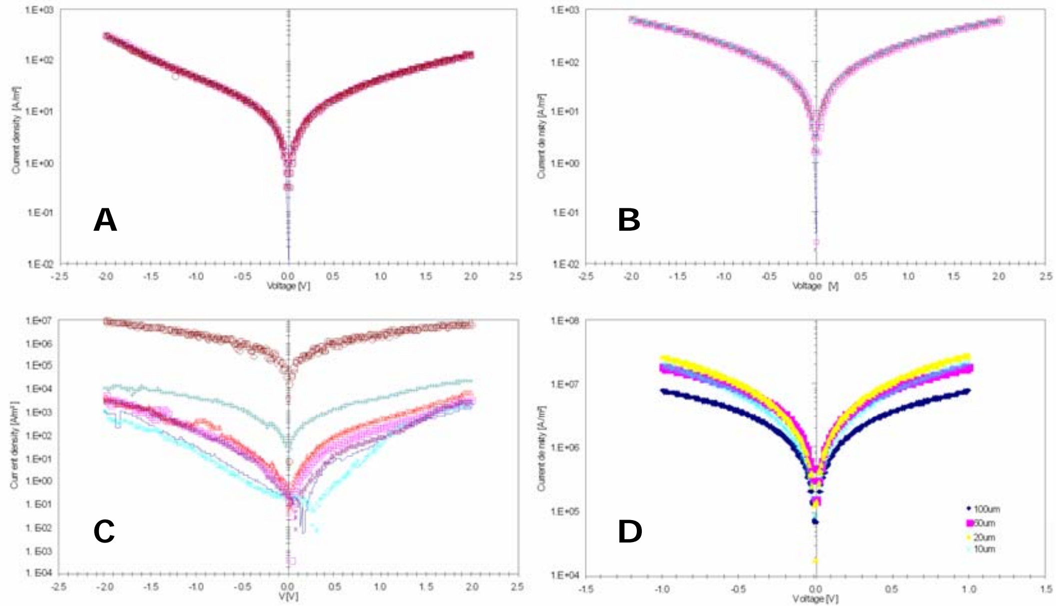

Figure 24 *Current density versus voltage characteristics of both MIMIM energy barriers. (a) Emitter barrier (SiO_2) 100 µm devices shows excellent scaling. (b) Emitter barrier (SiO_2) 60 µm devicesshows excellent scaling. (c) Emitter barrier (SiO_2) 20 µm devices shows reasonable scaling, 1 short. (d) Average current density versus voltage of the P4DT collector junctions. RS=$9.54*10^4$ ± $6.59*10^3$*

Appendix F : MIMIM symbol

For every electronic device a circuit symbol exists. Resistor, capacitor, voltage source, etc. all have a schematic representation to make drawing electronic circuits easy. In Figure 25 A and B we have shown the symbols of the well known bipolar junction transistor (BJT) and field effect transistor (FET).
The arrow in the circuit of the BJT is on the emitter leg and points in the direction of the conventional current flow. The graded well-shape depicts the energy well in the off-state of the transistor and the arrow also points in the direction of increasing carrier potential energy.
For the FET everything is somewhat different. The arrow points in the direction from P to N, so if the transistor has a P-channel it points in. The bending of the leads is again a potential well that shows the off-state of the device. With the gate the depth of the well can be decreased to connect the drain and source and switch the device on.
We used the principles from the symbols for the BJT and FET to design our own MIMIM symbol. Figure 25C shows the design. The two squares schematically represent the two barriers. The barrier heights should not be equal, but for simplicity of the symbol they are. The collector lead can be recognized by the arrow which indicates the conventional current flow. Note that although the MIMIM is very much like a BJT the arrow is not connected to the emitter lead. This is because we also wanted the arrow to point in the direction of increasing potential energy of the carriers.

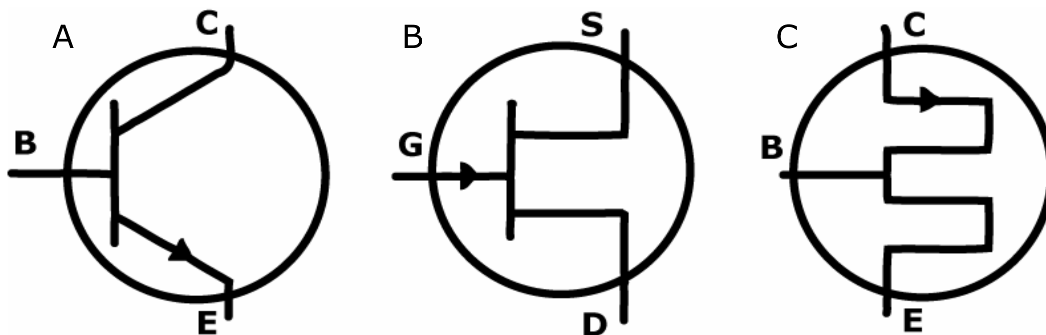

Figure 25 *(A) NPN bipolar junction transistor (BJT) symbol (B) N-channel field effect transistor (FET) symbol (C) metal-insulator-metal-insulator-metal transistor (MIMIM) symbol*